TECHNICAL MEMORANDUM

634

Ocean Wave effects on the daily cycle in SST

Peter A.E.M. Janssen

Research Department

12 October 2010

This paper has not been published and should be regarded as an Internal Report from ECMWF. Permission to quote from it should be obtained from the ECMWF.

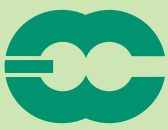

European Centre for Medium-Range Weather Forecasts
Europäisches Zentrum für mittelfristige Wettervorhersage
Centre européen pour les prévisions météorologiques à moyen terme

Series: ECMWF Technical Memoranda

A full list of ECMWF Publications can be found on our web site under:
http://www.ecmwf.int/publications/

Contact: library@ecmwf.int

©Copyright 2010

European Centre for Medium-Range Weather Forecasts
Shinfield Park, Reading, RG2 9AX, England

Literary and scientific copyrights belong to ECMWF and are reserved in all countries. This publication is not to be reprinted or translated in whole or in part without the written permission of the Director. Appropriate non-commercial use will normally be granted under the condition that reference is made to ECMWF.

The information within this publication is given in good faith and considered to be true, but ECMWF accepts no liability for error, omission and for loss or damage arising from its use.

Abstract

Ocean waves represent the interface between the ocean and the atmosphere, and, therefore, a wave model is needed to compute not only the wave spectrum, but is also required to determine the processes at the air-sea interface that govern the fluxes across the interface.

Here, starting from earlier results with the Turbulent Kinetic Energy Equation, a simple model is developed that allows for the inclusion of wave dissipation effects, effects of Langmuir turbulence and buoyancy on the simulation of the daily cycle in SST.

1 Introduction.

The work of Terray et al (1996) and Craig and Banner (1994) has highlighted the prominent role of breaking waves and its contribution to the surface current. In the field it is customary to find considerable deviations from the usual balance between production and dissipation of turbulent kinetic energy. These deviations are caused by the energy flux produced by surface wave damping. When observed turbulent kinetic energy dissipation, ε, and depth z are scaled by parameters related to the wave field, an almost universal relation between dimensionless dissipation and dimensionless depth is found. Here, dimensionless dissipation is given by $\varepsilon H_S/\Phi_{aw}$, with H_S the significant wave height and Φ_{aw} the energy flux from wind to waves, while the dimensionless depth is given by z/H_S.

The energy flux by surface wave damping is expected to affect the upper-ocean mixing up to a depth of the order of the significant wave height. Transport to the deeper layers of the ocean is possible because work against the shear in the Stokes drift generates Langmuir cells which have a penetration depth of the order of the inverse of a typical wave number of the wave field.

In this paper I would like to develop a multi-layer model of turbulent mixing in the upper ocean that includes effects of surface wave damping, Langmuir turbulence and stratification in addition to the usual shear production and dissipation. The model is applied to the problem of the evolution of the diurnal cycle in SST, and it is shown that, even for low wind speed, wave effects play an important role in determining the amplitude of the diurnal cycle.

The programme of the paper is as follows. In §2 a brief discussion of the role of ocean waves in air-sea interaction is given while it is shown how to obtain in a reliable way energy and momentum flux from the wave field. §3 gives some of the details of the mixed layer model that is proposed to describe the mixing processes in the upper ocean. The model consists of momentum equations and the heat equation. In the presence of turbulence these equations are not closed and the level-$2\frac{1}{2}$ Mellor-Yamada scheme is adopted to model the eddy viscosity for heat and momentum. These eddy viscosities are then found to depend on the turbulent kinetic energy (TKE) and hence the need for a TKE equation. In the present paper the TKE equation describes the rate of change of turbulent kinetic energy due to processes such as shear production (including shear in the Stokes drift), damping by buoyancy, vertical transport of pressure and TKE and dissipation of turbulence. It presents an ideal context to model effects of wave dissipation and Langmuir turbulence on the mixing properties of the upper ocean. In contrast to the Graig and Banner model effects of wave dissipation on mixing are taken into account by following the fairly novel approach of explicitely modelling the vertical transport of pressure in terms of the rate of change of the wave spectrum due to wave dissipation (A similar idea in the atmospheric context was pursued by Janssen (1999)). The effect of Langmuir turbulence, following Grant and Belcher (2009), is represented by the part in the shear production term that is connected to Stokes drift. The upper ocean may experience extremely stable conditions, especially during the day under low wind speed conditions; the modelling of these stable conditions therefore requires special attention. A model for buoyancy effects was developed which for weakly stable conditions is based on results from the Kansas field campaign (assuming

that atmospheric and oceanic turbulence behaves in a similar fashion) while the modelling of extremely stable conditions was guided by the renormalisation approach of Sukoriansky *et al.* (2005).

In §4 some properties of steady state solutions of the TKE equation are discussed. In particular, it is shown that to a good approximation diffusion of turbulent kinetic energy may be neglected. This approximation is called the *local* approximation because the turbulent kinetic energy then only depends on the local properties of the turbulent flow. In the local approximation it turns out that the TKE equation reduces to an algebraic problem and its solution indicates that the turbulent velocity (and hence the eddy viscosity) only weakly depends on the wave energy flux and the contribution by Langmuir turbulence (according to a 1/3-power law). Nevertheless, wave effects enhance the eddy viscosities by a factor of 2-3. Inspecting more closely the solution according to the local approximation it is found that wave dissipation affects the mixing process very close to the surface at a depth of the order of the significant wave height. Langmuir turbulence is found to affect mixing in the deeper parts of the upper ocean at a depth of the order of a typical wavelength of the ocean wave field. Also buoyancy effects are discussed in some detail. For weak stratification, the present model is shown to be in close agreement with the results of the Kansas field campaign (Businger *et al.*, 1971) while for extremely stable conditions it is found that momentum transport dominates heat transport, in agreement with Sukoriansky *et al.* (2005). In addition, the combined effects of waves and buoyancy are studied as well. It is found that under stable conditions buoyancy effects, which act in particular in the deeper parts of the upper ocean, suppress the effects of Langmuir turbulence. Finally, the TKE equation is shown to be in close agreement with the empirically known dependence of dimensionless turbulent dissipation on depth.

In §5 results of numerical simulations with the mixed layer model are presented. First, a synthetic example with constant momentum and heat fluxes is given, which is followed by a simulation of the sea surface temperature (SST) at a location in the Arabian Sea. The simulated diurnal cycle in SST is found to be in close agreement with in-situ observations. The importance of sea state effects, even for low wind speed cases, is shown as well. Finally, §6 gives a summary of conclusions.

2 Surface layer mixing and ocean waves.

In order to be able to give a realistic representation of the mixing processes in the surface layer of the ocean, it should be clear that a reliable estimate of energy and momentum fluxes to the ocean column is required. A first attempt to estimate these fluxes from modelled wave spectra and knowledge about the generation and dissipation of ocean waves was given by Komen (1987). Weber (1994) studied energy and momentum fluxes in the context of a low-resolution coupled ocean-wave atmosphere model (WAM-ECHAM), and it was concluded that there is no need to use a wave prediction model to determine the energy flux. A parametrization of the type $\Phi_{aw} = m\rho_a u_*^3$ (with u_* the air friction velocity and m a constant) would suffice. It will be shown here that this conclusion depends on an approximation used by Weber to estimate the energy flux.

As energy and momentum flux depend on the spectral shape, the solution of the energy balance equation is required. It reads

$$\frac{\partial}{\partial t}F + \mathbf{v}_g . \frac{\partial}{\partial \mathbf{x}}F = S_{in} + S_{nl} + S_{diss} + S_{bot}, \tag{1}$$

where $F = F(\omega, \theta)$ is the two-dimensional wave spectrum which gives the energy distribution of the ocean waves over angular frequency ω and propagation direction θ. Furthermore, $\mathbf{v}_g$ is the group velocity and on the right hand side there are four source terms. The first one, S_{in} describes the generation of ocean waves by wind and therefore represents the momentum and energy transfer from air to ocean waves. The third and fourth term describe the dissipation of waves by processes such as white-capping, large scale breaking eddy-induced damping and bottom friction, while the second terms denotes nonlinear transfer by resonant four-wave

interactions. The nonlinear transfer conserves total energy and momentum and is important in shaping the wave spectrum and in the down-shift towards lower frequencies.

Let us first define the momentum and energy flux. The total wave momentum **P** depends on the variance spectrum $F(\omega,\theta)$ and is defined as

$$\mathbf{P} = \rho_w g \int_0^{2\pi} \int_0^{\infty} d\omega d\theta \, \frac{\mathbf{k}}{\omega} F(\omega,\theta), \tag{2}$$

which agrees with the well-known relation that wave momentum is simply wave energy divided by the phase speed of the waves. The momentum fluxes to and from the wave field are given by the rate of change in time of wave momentum, and one may distinguish different momentum fluxes depending on the different physical processes. For example, making use of the energy balance equation (1) the wave-induced stress is given by

$$\tau_{aw} = \rho_w g \int_0^{2\pi} \int_0^{\infty} d\omega d\theta \, \frac{\mathbf{k}}{\omega} S_{in}(\omega,\theta), \tag{3}$$

while the dissipation stress is given by

$$\tau_{wo} = \rho_w g \int_0^{2\pi} \int_0^{\infty} d\omega d\theta \, \frac{\mathbf{k}}{\omega} S_{diss}(\omega,\theta), \tag{4}$$

Similarly, the energy flux from wind to waves is defined by

$$\Phi_{aw} = \rho_w g \int_0^{2\pi} \int_0^{\infty} d\omega d\theta \, S_{in}(\omega,\theta), \tag{5}$$

and the definition for the energy flux from waves to ocean, Φ_{wo}, follows immediately from the above one by replacing S_{in} by S_{diss}. It is important to note that while the momentum fluxes are mainly determined by the high-frequency part of the wave spectrum, the energy flux is to a larger extent determined by the low-frequency waves.

In an operational wave model, the prognostic frequency range is limited by practical considerations such as restrictions on computation time, but also by the consideration that the high-frequency part of the dissipation source function is not well-known. In the ECMWF version of the WAM model the prognostic range of the wave spectrum is given by the condition

$$\omega < \omega_c = \max(2.5\omega_{mean}, 4\omega_{pm}) \tag{6}$$

where ω_{mean} is a conveniently defined mean angular frequency and ω_{pm} is the Pierson Moskovitch frequency. In the diagnostic range, $\omega > \omega_c$, the wave spectrum is given by Phillips' ω^{-5} power law. In the diagnostic range it is assumed that there is a balance between wind input, dissipation and nonlinear transfer. In practice this means that all energy and momentum going into the high-frequency range of the spectrum is dissipated, and is therefore directly transferred to the ocean column.

As a consequence, the momentum flux to the ocean, τ_{oc}, is given by

$$\tau_{oc} = \tau_a - \rho_w g \int_0^{2\pi} \int_0^{\omega_c} d\omega d\theta \, \frac{\mathbf{k}}{\omega} \left(S_{in} + S_{nl} + S_{diss}\right), \tag{7}$$

where τ_a is the atmospheric stress, whose magnitude is given by $\tau_a = \rho_a u_*^2$. Note that the ocean momentum flux τ_{oc} only involves the sum of the three source functions of the energy balance equation and therefore it only involves the total rate of change of wave momentum. Any wave model that is forced by reliable atmospheric stresses and that produces wave height results that compare well with, for example, buoy wave height data and Altimeter wave height data, will produce reliable estimates of the ocean momentum flux τ_{oc}.

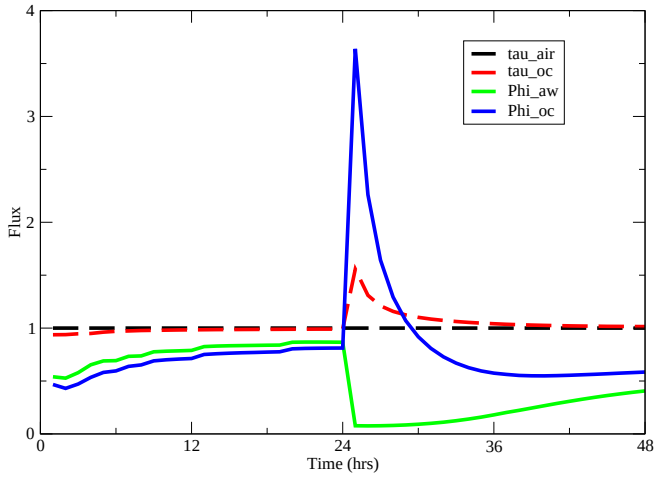

Figure 1: Evolution in time of normalized momentum flux and energy flux to the ocean for the case of a passing front after 24 hrs. The momentum flux has been normalized with $\rho_a u_*^2$, while the energy flux has been normalized with $m\rho_a u_*^3$, where $m = 5.2$.

Ignoring the direct energy flux from air to currents, because it is small (cf. Phillips, 1977), the energy flux to the ocean, Φ_{oc}, is given by

$$\Phi_{oc} = \Phi_{aw}^{tot} - \rho_w g \int_0^{2\pi} \int_0^{\omega_c} d\omega d\theta \; (S_{in} + S_{nl} + S_{diss}) \,, \tag{8}$$

where Φ_{aw}^{tot} is the total energy flux transferred from air to ocean waves. This total energy flux is fairly well-known, because empirically the wind input to ocean waves is well-known, even in the high-frequency part of the spectrum (cf. Plant, 1982). Furthermore, there is now a consensus that the high-frequency part of the spectrum obeys an ω^{-5} power law (Banner, 1990; Birch and Ewing, 1986; Hara and Karachintsev, 2003, to mention but a few references). Hence, fairly reliable estimates of the energy flux Φ_{oc} may be provided by means of a wave model provided the model has a wind input term that agrees with the observations of wave growth and provided modelled wave heights compare well with observations.

Before results of time series for momentum and energy flux for a simple case are presented, we have to make one remark on the numerical implementation of (4) and (5). The energy balance equation is solved by means of an implicit integration scheme (cf. Komen et al, 1994). To be consistent with the numerical treatment of the energy balance, the momentum and energy flux have to be treated in a similar spirit, i.e. including the implicit factors of the integration scheme.

Let us now illustrate the sea-state dependence of the momentum and energy flux for the simple case of the passage of a front. To that end we take a single grid-point version of the ECMWF version of the WAM model and force the waves for the first day with a constant wind speed of 18 m/s, which is followed by a drop in wind speed to 10 m/s and a change in wind direction by 90 deg. In Fig. 1 we have plotted time series of atmospheric stress (τ_a), the momentum flux to the ocean (τ_{oc}), the total air-wave energy flux (Φ_{aw}^{tot}) and the energy flux into the ocean (Φ_{oc}). The momentum fluxes have been normalized by τ_a, while the energy fluxes have been normalized by $m\rho_a u_*^3$, with $m = 5.2$ which is a convenient mean value. During the first day we deal with the case of wind-generated gravity waves, hence windsea, and, in particular, the difference between atmospheric stress and the momentum flux to the ocean is small, most of the time at best 2%. This is a well-known property of windsea (JONSWAP, 1973). For windsea, the difference between total energy flux Φ_{aw}^{tot} and the energy flux

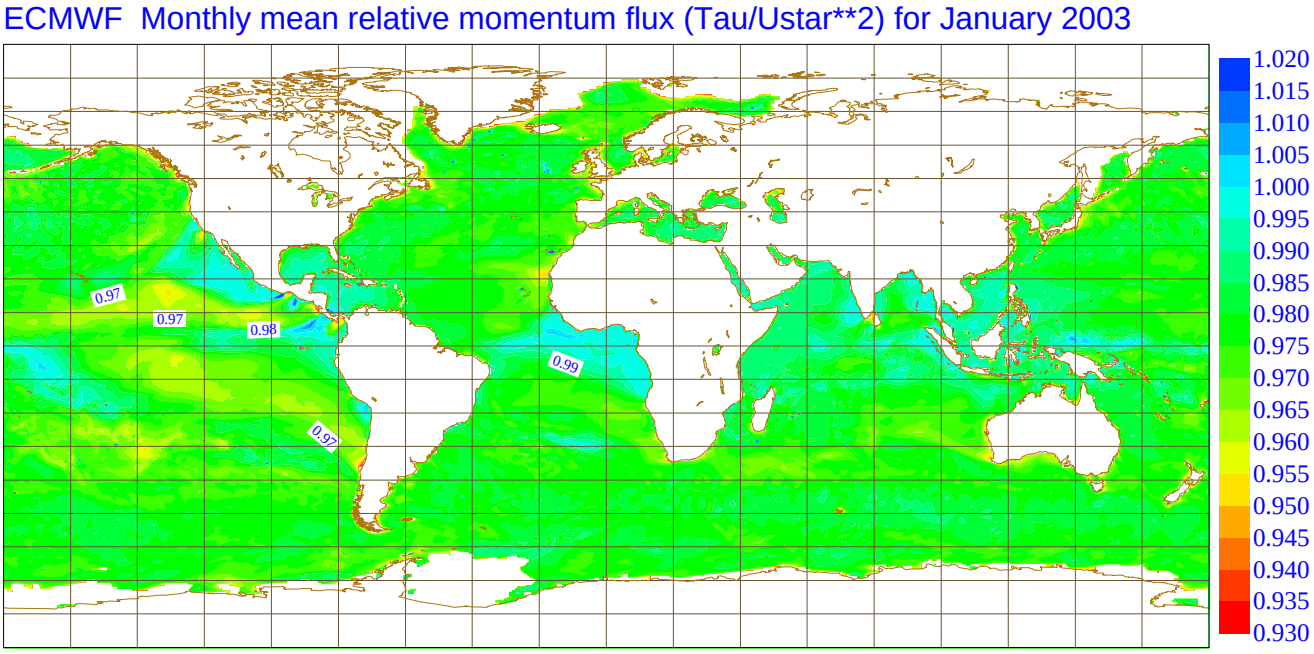

Figure 2: Monthly mean of momentum flux into the ocean, normalized with the atmospheric stress. Period is January 2003.

into the ocean Φ_{oc} is somewhat larger. When the front passes at $T = 24\,hrs$ there is a sudden drop in wind, hence in atmospheric stress. However, the waves are still steep and experience an excessive amount of dissipation in such a way that wave energy decreases. As a consequence, considerable amounts of momentum and energy are dumped in the ocean column, much larger than the amounts one would expect from the local wind. Therefore, in cases of rapidly varying circumstances, the fluxes are seen to depend on the sea state. This is in particular true for the energy flux Φ_{oc} and to a much lesser extent for the momentum flux τ_{oc}.

This different behaviour of momentum flux and energy flux is caused by a combination of two factors. By definition momentum flux is mainly determined by the high frequency part of the spectrum while we have assumed that in the unresolved part of the spectrum there is a balance between wind input and dissipation. Hence, for windsea there is almost always a balance between atmospheric momentum flux and the flux into the ocean. This holds to a lesser extent for the energy flux because this flux is partly determined by the low frequency part of the wave spectrum as well.

The different behaviour of momentum and energy flux is also found in the monthly means on a global scale. This is illustrated in the Figs. 2 and 3, which are taken from Janssen *et al.* (2004). The typical variation in the ratio τ_{oc}/τ_a is then found to be of the order of 4% while the variation in the normalized energy flux, $\Phi_{oc}/m\rho_a u_*^3$, is substantially larger. The global average of the value for m turns out to be $m \simeq 5.2$. Note that the map for the energy flux shows an interesting spatial pattern. In the equatorial region values of the normalized energy flux are small, suggesting that the mixed layer is thinner than the norm. In the extra-Tropics the normalized energy flux is considerably larger, presumably because here there is larger variability in the wind field.

We finally remark that in the work of Weber (1994) the energy flux into the ocean was approximated by the relation $\Phi_{oc} \simeq \langle c \rangle \tau_{aw}$, where $\langle c \rangle$ is the mean phase velocity. This generally overestimates the energy flux by at least a factor of two and as a consequence fairly high values of m ($m \simeq 14$) are found. In addition, in interesting cases such as the passage of a front, the energy flux approximated in this manner will follow the wind. For example, in the frontal case of Fig. 1 the energy flux to the ocean would decrease dramatically at $T = 24$ hrs, while, in fact, it should hardly change. Therefore, it is not surprising that with this approximation the energy

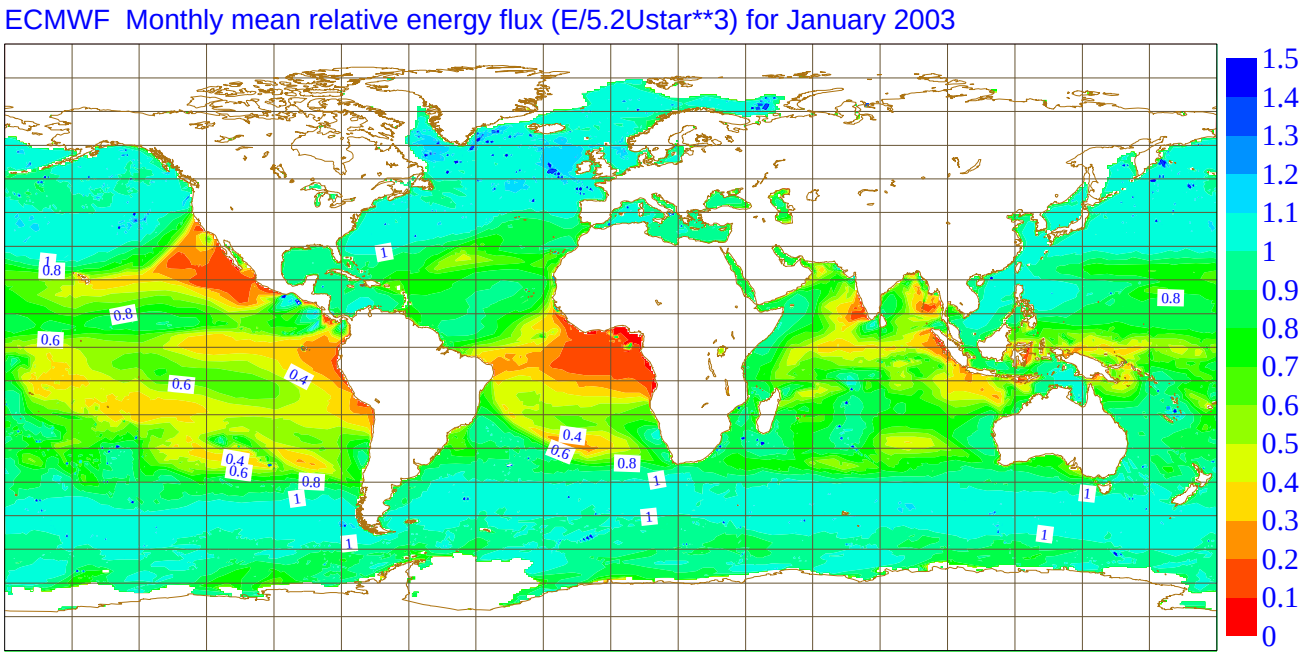

Figure 3: Monthly mean of energy flux into the ocean, normalized with $m\rho_a u_*^3$ where $m \simeq 5.2$. Period is January 2003.

flux Φ_{oc} and wind are closely related.

It is concluded that it is not a good idea to estimate the energy flux from the local stress, because significant memory effects are present in rapidly varying circumstances. In general, when wave information is available, it is preferred to directly use knowledge on the evolution of the sea state due to wave dissipation, c.f. Eq. (8). Furthermore, on average 98% of the atmospheric stress is transferred locally to the ocean, while 2% of the wave momentum is advected away and finally dissipates at the shores. However, under extreme circumstances such as during hurricanes as much as 10% of the wave momentum may be advected away. Therefore, although on average differences are small, it seems preferable to drive the ocean with the momentum flux from waves to ocean, cf. Eq. (7), because the alternative choice would introduce slightly more momentum in the ocean colum, which in long integrations may give a contribution to climate drift.

3 Mixed layer modelling.

Having found a reliable way of obtaining from the rate of change of the wave spectrum the momentum and energy flux into the ocean, we now turn our attention to the consequences for the mean flow in the ocean. We start from the work of Craig and Banner (1994) (and Mellor and Yamada (1982)) who introduced effects of wave dissipation on turbulent mixing by specifying the energy flux at the surface as a surface boundary condition to the turbulent kinetic energy (TKE) equation. Following Grant and Belcher (2009), the TKE equation is extended by introducing the generation of Langmuir circulation through work done against the shear in the Stokes drift. Furthermore, following Noh and Kim (1999) and Baas *et al.* (2008), the important effects of buoyancy are introduced as well. We discuss the consequences for the momentum and heat equation, where the eddy viscosity is expressed as a product of a mixing length and turbulent velocity which follows from the solution of the turbulent kinetic energy budget.

The model is applied to the problem of the diurnal cycle in sea surface temperature (SST), which is quite a challenge because the SST follows from a balance between absorption of solar radiation in water and turbulent

transport of heat. Assuming that the amplitude of the diurnal cycle can be measured accurately and since the absorption profile of solar radiation is well-known, this application provides a sensitive test of our ideas of mixing in the upper ocean. In this Section the model is presented, while in §4 the properties of the steady state version of the momentum, heat and TKE equations are studied. This is then followed in §5 by applying the dynamical model to a synthetic case of constant wind forcing and heat flux, while, using observed forcings, the model is also applied to simulate the diurnal cycle in subsurface temperature for a three month period in the Arabian Sea.

3.1 Momentum equation.

To simplify the problem, the wind/wave driven water velocity is assumed to be non-rotating and uniform without any pressure gradients in the horizontal directions. For convenience increasing depth is taken in the positive z-direction. The momentum equation then reduces to

$$\frac{\partial u}{\partial t} = -\frac{\partial \tau}{\partial z},\ \tau = -\langle \delta u \delta w \rangle, \tag{9}$$

where τ is the stress in the water column which is usually parametrized as $\tau = -\nu \partial u/\partial z$, assuming that the main component of the water velocity is turbulent. However, in the same spirit as done for the problem of wind wave generation (Janssen, 1999; Janssen *et al.*, 2004) it is suggested that in particular in the upper part of the ocean column wave motion is an important component as well. Therefore, the fluctuating parts of the velocity are written as a sum of wave-induced motion, denoted with a subscript w, and turbulent motion, denoted with a prime $'$, and it is assumed that there is no correlation between wave motion and turbulence. As a result the stress τ becomes

$$\tau = -\langle \delta u_w \delta w_w \rangle - \langle u' w' \rangle,$$

and the turbulent part of the stress is modelled with a mixing length model while the wave-induced part is given, i.e. independent of the current. The shape of the wave-induced stress is prescribed by a function whose derivative vanishes at the surface[1], hence

$$-\langle \delta u_w \delta w_w \rangle = \frac{\tau_{oc}}{\rho_w} \times \hat{T}(z),\ 1 - \hat{T}(z) = (1 - e^{-z/z_0})^2,$$

where z_0 determines the gradient of the wave-induced stress and is considered to be closely related to the significant wave height H_S. In other words, it is assumed that wave dissipation affects at most a layer of thickness of the wave height. Combining everything together and introducing the water friction velocity w_* according to

$$\tau_{oc} = \rho_w w_*^2 \tag{10}$$

the momentum equation becomes

$$\frac{\partial u}{\partial t} = \frac{\partial}{\partial z}\left(\nu_m \frac{\partial u}{\partial z}\right) - w_*^2 \frac{d\hat{T}(z)}{dz}. \tag{11}$$

Here, ν_m is the eddy viscosity for momentum and following Craig and Banner (1994) the level-$2\frac{1}{2}$ Mellor-Yamada scheme is used (Mellor and Yamada, 1982). Hence, the eddy viscosity for momentum (and heat denoted by ν_h) is expressed as

$$\nu_{m,h} = l(z) q(z) S_{M,H} \tag{12}$$

[1] the reason for the vanishing of the first derivative will be explained shortly

where $l(z)$ is the turbulent mixing length, $e = q^2/2$ is the turbulent kinetic energy ($q(z)$ is referred to as the turbulent velocity) and S_M and S_H are dimensionless parameters which may still depend on stratification. The turbulent velocity q will be obtained from the TKE equation, while the expression for the mixing length will be introduced during the discussion of buoyancy effects.

Eq. (11) is the basic evolution equation for the ocean current. In order to better understand the role of the wave-induced stress profile it is of interest to study the case of a time-independent current. Then, the momentum equation becomes

$$\frac{d}{dz}\left(\nu_m \frac{du}{dz}\right) - w_*^2 \frac{d\hat{T}(z)}{dz} = 0.$$

Integrating once with respect to depth and realizing that the momentum flux to the water column is suplied entirely by surface wave dissipation one finds

$$\nu_m \frac{du}{dz} = -w_*^2 \left(1 - \hat{T}(z)\right).$$

and this equation can be immediately integrated for u with the result

$$u = -w_*^2 \int_H^z \mathrm{d}z \frac{1 - \hat{T}(z)}{\nu_m}. \tag{13}$$

The advantage of the introduction of the wave-induced profile is now immediately evident by closer inspection of the relation (13). In the usual approach the function $\hat{T}$ is absent and if one would choose an eddy viscosity which is a linear function of depth or height a logarithmic singularity would occur upon evaluation of the integral. This singularity can only be avoided by the introduction of a 'mysterious' roughness length z_0. In the present case such an 'ad-hoc' measure is not needed. Now, the integrand has no singularity at the origin because the function $1 - \hat{T}(z)$ vanishes sufficiently rapidly near the surface therefore cancelling the singularity caused by the eddy-viscosity ν in the denominator. Therefore, in the following the eddy viscosity is assumed to be given by Eq. (12), while the mixing length scale $l(z)$ is assumed to vanish for $z \to 0$.

Remark: One may apply a similar reasoning to the problem of air flow over wind-generated gravity waves. The wave-induced stress is then determined by the wind-input source function, and the wind profile follows from

$$\nu_m \frac{dU}{dz} = u_*^2 \left(1 - \hat{T}(z)\right).$$

The eddy-viscosity ν_m is again given by Eq. (12), i.e. $\nu_m = l(z)q(z)S_M$. The turbulent velocity $q(z)$ is obtained from the kinetic energy equation, and for simplicity I assume that this consists of a balance between production and dissipation. This implies

$$\nu_m \left(\frac{dU}{dz}\right)^2 = \varepsilon$$

where the dissipation $\varepsilon = q^3/Bl$. Making use of the expression for the eddy viscosity in the energy budget, the turbulent velocity is readily found and, as a result the eddy viscosity becomes

$$\nu_m = l^2(z)\left|\frac{dU}{dz}\right|$$

where the relation $B^{1/4}S_M^{3/4} = 1$ is used. Substitution of the eddy viscosity in the momentum equation finally gives for the wind profile

$$U(z) = u_* \int_0^z \frac{\mathrm{d}z}{l(z)} \left(1 - \hat{T}(z)\right)^{1/2},$$

for the boundary condition that the wind velocity vanishes at the surface. Now, taking as mixing length $l(z) = \kappa z$ it is immediately evident from the above expression that the wind velocity only remains finite provided $1 - \hat{T}(z) \sim z^2$ for vanishing height z. Therefore, choosing for the stress profile

$$\left(1 - \hat{T}(z)\right)^{1/2} = 1 - e^{-z/z_0},$$

the expression for the wind profile U becomes

$$U(z) = u_*/\kappa \int_0^z \frac{\mathrm{d}z}{z} \left(1 - e^{-z/z_0}\right).$$

The integral may be expressed in terms of the exponential integral $E_1(z)$ (see Abramowitz and Stegun, 1964), hence,

$$U(z) = \frac{u_*}{\kappa} \left[\log(z/z_0) + \gamma + E_1(z/z_0)\right],$$

where $\gamma = 0.57721$ is Euler's constant. Expressions for $E_1(z)$ for small and large z are known. The resulting form of the wind profile for small z/z_0 becomes

$$U(z) \approx \frac{u_*}{\kappa} \frac{z}{z_0},$$

while for large z/z_0 the wind profile becomes

$$U(z) \approx \frac{u_*}{\kappa} \log(z/y_0),\ y_0 = e^{-\gamma} z_0.$$

Remarkably, as $e^{-\gamma} \approx 0.561$, the outer flow experiences a smoother flow than the inner flow.

In summary, the roughness length may be explained in terms of a gradient length related to the wave-induced stress profile $\hat{T}(z)$. However, in order to obtain a finite surface velocity there are restrictions to the behaviour of the wave stress profile near the surface, $1 - \hat{T}(z) \sim z^2$!

3.2 Heat equation.

The heat equation describes the evolution of the temperature T due to radiative forcing and turbulent diffusion. Using the depth variable z, the temperature evolves according to

$$\frac{\partial T}{\partial t} = -\frac{1}{\rho_w c_w} \frac{\partial R}{\partial z} + \frac{\partial}{\partial z} \nu_h \frac{\partial T}{\partial z}, \tag{14}$$

where ν_h is the eddy viscosity for heat, given by Eq. (12), while the solar radiation profile $R(z)$ is parametrized following the work of Soloviev (1982), i.e.

$$R(z) = a_1 \exp(-z/z_1) + a_2 \exp(-z/z_2) + a_3 \exp(-z/z_3) \tag{15}$$

with

$$(a_1, a_2, a_3) = (0.28, 0.27, 0.45)$$

while

$$(z_1, z_2, z_3) = (0.013986, 0.357143, 14.28571).$$

The decay length scale z_1, corresponding to the absorption of light in the near UV range, is seen to be quite small, of the order of 1 cm. Therefore, in order to capture the absorption of light in the near UV range high resolution in z near the ocean surface is required.

The 'turbulent' heat transport could have been modelled in a similar fashion as done for the momentum equation by adding a explicit contribution due to the presence of growing water waves. So far this has not been done yet.

3.3 Kinetic energy equation.

The equation for the kinetic energy of the turbulent velocity fluctuations is obtained from the Navier-Stokes equations. If effects of advection are ignored, the TKE equation describes the rate of change of turbulent kinetic energy e due to processes such as shear production (including the shear in the Stokes drift), damping by buoyancy, vertical transport of pressure and TKE, and turbulent dissipation ε. It reads

$$\frac{\partial e}{\partial t} = \nu_m S^2 + \nu_m S \frac{\partial U_S}{\partial z} - \nu_h N^2 + \frac{1}{\rho_w}\frac{\partial}{\partial z}(\overline{\delta p \delta w}) + \frac{\partial}{\partial z}(\overline{e\delta w}) - \varepsilon, \tag{16}$$

where $e = q^2/2$, with q the turbulent velocity, $S = \partial U/\partial z$ and $N^2 = g\rho_0^{-1}\partial\rho/\partial z$, with N the Brunt-Väisälä frequency, ρ_w is the water density, δp and δw are the pressure and vertical velocity fluctuations and the over-bar denotes an average taken over a time scale that removes linear turbulent fluctuations

The turbulent production by Langmuir circulation is modelled following Grant and Belcher (2009) by the second term on the right-hand side of Eq. (16) which represents works against the shear in the Stokes drift. Here U_S is the magnitude of the Stokes drift for a general wave spectrum $F(\omega)$,

$$U_S = \frac{2}{g}\int_0^\infty d\omega\, \omega^3 F(\omega) e^{-2k|z|},\ k = \omega^2/g.$$

Although in principle the depth dependence of the Stokes drift is known it still is a fairly elaborate expression through the above integral. In the final result we will use the approximate expression

$$U_S = U_S(0)e^{-2k_S z},$$

where $U_S(0)$ is the value of the Stokes drift at the surface and k_S is an appropiately chosen wavenumber scale.

The dissipation term is taken to be proportional to the cube of the turbulent velocity divided by the mixing length

$$\varepsilon = \frac{q^3}{Bl}, \tag{17}$$

Here, B is another dimensionless constant.

It is customary (see e.g. Mellor and Yamada, 1982) to model the combined effects of the pressure term and the vertical transport of TKE by means of a diffusion term. Thus,

$$\frac{1}{\rho_w}\frac{\partial}{\partial z}(\overline{\delta p \delta w}) + \frac{\partial}{\partial z}(\overline{e\delta w}) = \frac{\partial}{\partial z}\left(lqS_q\frac{\partial e}{\partial z}\right)$$

where S_q is a constant. As a result the TKE equation becomes

$$\frac{\partial e}{\partial t} = \frac{\partial}{\partial z}\left(lqS_q\frac{\partial e}{\partial z}\right) + \nu_m S^2 - w_*^2\frac{\partial U_S}{\partial z} - \nu_h N^2 - 2\sqrt{2}\frac{e^{3/2}}{Bl(z)},$$

and this equation has to be supplemented by boundary conditions. Following Craig and Banner (1994) it is often assumed that the energy flux at the surface is supplied by wave dissipation. Hence the boundary condition at the surface becomes

$$-lqS_q\frac{\partial e}{\partial z} = F_0 \qquad \text{for} \qquad z = 0,$$

while at infinite depth the gradient in TKE is assumed to vanish,

$$\frac{\partial e}{\partial z} = 0 \qquad \text{for} \qquad z \to \infty.$$

The energy flux $\rho_w F_0$ is related to the energy flux into the ocean by

$$\rho_w F_0 = \Phi oc \tag{18}$$

where Φoc is the energy flux by breaking and/or dissipating waves given by Eq. (8). In the absence of the relevant information on the sea state, the energy flux is often parametrized as $\Phi oc = m\rho_a u_*^3$. Hence writing,

$$F_0 = \alpha w_*^3, \tag{19}$$

one then finds $\alpha = m(\rho_w/\rho_a)^{1/2}$. With m in the range of $2-10$, α has typical values of the order $50-250$. Using a wave prediction system m and α can be determined explicitely.

However, the pressure term can also be determined by explicitely modelling the energy transport caused by wave dissipation. Janssen (1999) demonstrated how the pressure term may affect flow in the atmospheric boundary layer by explicitely using knowledge on the growth of waves by wind. The same idea will be used here (cf. Janssen *et al.* (2004)) but now applied to wave dissipation in the ocean column. The correlation between pressure fluctuation and vertical velocity fluctuation at the surface is

$$I_w(0) = +\frac{1}{\rho_w}\overline{\delta p \delta w}(z=0) = g\int_0^\infty S_{diss}(\mathbf{k})d\mathbf{k} \tag{20}$$

and the main problem is how to model the depth dependence of $\overline{\delta p \delta w}$. One could perhaps argue that the depth dependence may be modelled in a similar way as the depth dependence of the Stokes drift (i.e. assume potential flow with the usual $\exp(-2kz)$ factor inside the integral), but I would expect that the main action of wave dissipation is in a layer of thickness of the wave height H_S. However, it is emphasized that there are still a number of open questions regarding the nature of surface wave dissipation. The suggested causes of the wave dissipation range from large scale wave breaking to microscale breaking or even by ocean eddies generated by unsteady large scale waves. Each different process will have a different penetration depth and for simplicity it is assumed here that these lengthscales can all be lumped together to one wave height scale. Therefore the following depth dependence for $I(z)$ is suggested:

$$I_w(z) = +\frac{1}{\rho_w}\overline{\delta p \delta w} = I_w(0)\times \hat{I}_w,\ \hat{I}_w = e^{-z/z_0} \tag{21}$$

where the depth scale $z_0 \sim H_S$ will play the role of a roughness length. The surface value of I_w may be obtained from Eq. (19), realizing that by definition I_w is negative, hence

$$I_w(0) = -\alpha w_*^3 \tag{22}$$

Using Eq. (21) in (16) the TKE equation becomes

$$\frac{\partial e}{\partial t} = \frac{\partial}{\partial z}\left(lqS_q\frac{\partial e}{\partial z}\right) + \frac{\partial I_w(z)}{\partial z} + \nu_m S^2 - w_*^2\frac{\partial U_S}{\partial z} - \nu_h N^2 - \frac{2\sqrt{2}}{Bl(z)}e^{3/2}. \tag{23}$$

At the surface there is no direct conversion of mechanical energy to turbulent energy and therefore the flux of turbulent energy is assumed to vanish. Hence the boundary conditions become

$$lqS_q\frac{\partial e}{\partial z} = 0 \qquad \text{for} \qquad z=0, \tag{24}$$

$$\frac{\partial e}{\partial z} = 0 \qquad \text{for} \qquad z\to\infty. \tag{25}$$

The values used in the empirical constants are from the Mellor-Yamada model. They are

$$(S_M, S_q, B) = (0.39, 0.2, 16.6) \tag{26}$$

Note that in order to agree with the turbulence results in case there is a balance between production and dissipation of kinetic energy the parameters S_M and B satisfy the relation $B^{1/4}S_M^{3/4} = 1$.

3.3.1 *Buoyancy and the mixing length $l(z)$.*

The description of the TKE equation is concluded by means of a discussion of buoyancy effects and the choice of the mixing length. In the upper ocean effects of stratification are important. In this paper the present mixed layer model will be applied to the prediction of the diurnal cycle in SST. Extreme events typically arise for low winds. At sunrise the upper ocean is usually neutrally stably stratified and the temperature profile is almost uniform. When the sun starts shining the top layer of the ocean gets heated up resulting in stable conditions which reduce the heat transport to the layers below. As a consequence a considerable amount of heat is retained in the top layer which may have a thickness of a few decimeters only. In the course of the day more and more heat is added to this top layer with the consequence that the layer becomes more and more stable, reducing heat transport to the layers below even more. In the extreme circumstances of low winds of 1 m/s the Obukhov length may go down to a few centimetres, which is much smaller then what is encountered in the atmospheric case. An adequate modelling of these extremely stable cases is clearly of the utmost importance, but little empirical evidence is available for these extreme circumstances. Notable exceptions are the works of Cheng and Brutsaert (2005) and of Grachev *et al.* (2007).

In the presence of stable stratification it may be argued that buoyancy gives rise to a reduction of momentum and heat transport, because when the Richardson number would pass $1/4$ then fluid motion will be damped. Following Csanady (1964), Deardorff (1980), Britter *et al.* (1983) and Wyngaard (1985), this means that there is an additional parameter which may determine the transport properties of the upper ocean, namely the Brunt-Väisälä frequency N. Under very stable conditions one would expect that most of the 'turbulent' energy is concentrated near N which suggests that the mixing length is limited by an additional length scale $l_b = q/N$. The eddy viscosity can then be estimated by

$$\nu \sim q l_b \sim q l R i_t^{-1/2} \tag{27}$$

where

$$Ri_t = (Nl/q)^2 \tag{28}$$

is the Richardson number for turbulent eddies and the mixing length l is chosen as the usual one for neutrally stable flow, i.e.

$$l(z) = \kappa z \tag{29}$$

with $\kappa = 0.4$ the von Kármán constant. On the basis of Eq. (27) which is valid at large Ri_t, Noh and Kim (1999)[2] suggested that the dimensionless parameters $S_{M,H}$ can be represented by

$$S_{M,H}/S_0 = f_{M,H}(Ri_t);\ f_{M,H} = a_{M,H}(1 + b_{M,H} Ri_t)^{-1/2} + c_{M,H} \tag{30}$$

with $a_{M,H}$, $b_{M,H}$ and $c_{M,H}$ empirical constants. In fact, Noh and Kim (1999) have chosen zero values of $c_{M,H}$, but a number of studies have suggested that at least S_M should have a finite value of c_M in order to represent effects of internal waves on momentum transport (Pacanowski and Philander, 1981; Strang and Fernando, 2001; Sukoriansky *et al.* 2005). Finite c_M has important consequences for the turbulent transport properties: while for zero c_M there is a critical value of the gradient Richardson number above which there is no transport, in case of finite values of c_M a critical Richardson number does not exist in agreement with the notion that also internal waves may give rise to momentum transport. Furthermore, also the diffusion of turbulent kinetic energy

[2] Baas *et al.* (2008) followed a similar idea but rather than modifying the parameters $S_{M,H}$ they modified the mixing length directly by assuming $l = l(\kappa z, l_b)$. But by inspection of (12) it is realized that this amounts to the same thing.

is expected to be affected by effects of stratification as the size of the eddies is limited under strongly stable circumstances. And the same applies to the coefficient B in the dissipation. As a consequence

$$S_q/S_{q0} = B/B_0 = f_M(Ri_t)$$

thus under stable conditions the TKE transport enjoys the same reduction as the momentum transport. The coefficients S_0, S_{q0} and B_0 assume the values as given in Eq. (26).

Finally, the case of unstable stratification ($Ri_t < 0$) needs to be modelled properly as well. It is assumed that also in this case the relevant parameters depend on the turbulent Richardson number Ri_t but the functional dependence is different. In this paper the following form is chosen for $f_{M,H}$ if $Ri_t < 0$:

$$f_{M,H} = (a_{M,H} + c_{M,H})(1 + \frac{d_{M,H} Ri_t}{1 + d_{M,H} Ri_t}$$

where $d_{M,H} = -20$ and $f_{M,H}$ is continuous at $Ri_t = 0$ while for $Ri_t \to -\infty$ the dimensionless parameter $f_{M,H}$ is twice as large as its value at the origin. Although not shown explicitely here, this choice results in good agreement with the parametrizations of dimensionless shear function and virtual potential temperature gradient obtained from the Kansas field campaign (Businger *et al.*, 1971). However, the experience from simulations of the diurnal cycle suggests that the evolution of sea surface temperature and surface current is fairly insensitive to details of how transport in unstable circumstances is represented.

4 Some properties of the TKE equation.

In §3 the mixed layer model has been described and it is straightforward to solve these equations numerically (see e.g. Kondo *et al.*, 1979, Mellor and Yamada, 1982, and Noh and Kim, 1999). Here, some interesting properties of the TKE equation will be discussed, in particular regarding effects of ocean waves on turbulent transport and effects of buoyancy. The discussion will be restricted to the steady state case.

Consider the steady state version of the TKE equation and eliminate the shear S and the buoyancy frequency N using the equations for momentum (11) and heat (14). From (11) one obtains for the shear

$$\nu_m S = -w_*^2 \left(1 - \hat{T}\right)$$

Similarly, integrating (14) once with respect to depth z and prescibing the heat flux Q_h at the surface one finds

$$\nu_h \frac{\partial T}{\partial z} = -\frac{Q_h + R(0) - R(z)}{\rho_w c_p}$$

In order to eliminate the buoyancy frequency $N = g\rho'/\rho$ it is assumed that the water density is a function of temperature only, hence $\rho = \rho(T)$ and therefore the vertical gradient in density can be connected to the temperature gradient through the thermal expansion coefficient α_w, i.e.

$$\frac{1}{\rho}\frac{\partial \rho}{\partial z} = -\alpha_w \frac{\partial T}{\partial z}.$$

Next, one introduces the dimensionless turbulent velocity Q,

$$q = w_* \left(\frac{B}{S_M}\right)^{1/4} Q \qquad \text{and} \qquad w = Q^3. \tag{31}$$

Furthermore, introduce a new length scale x,

$$dx = \frac{dz}{l\sqrt{\frac{1}{3}S_q B}} \qquad \Rightarrow \qquad x = \int \frac{dz}{l\sqrt{\frac{1}{3}S_q B}} \tag{32}$$

where it is noted that the range of the new variable x is from $-\infty$ to ∞ because the turbulent mixing length $l(z) = \kappa z$ vanishes at the surface. The TKE equation (23) then assumes the simple form

$$\frac{d^2 w}{dx^2} - w + \left(1 - \hat{T}\right)^2 w^{-1/3} - \zeta f_M = S(x), \tag{33}$$

where the source function reads

$$S(x) = \Phi_0 \frac{d\hat{I}_w}{dx} + \mu La^{-2}\left(1 - \hat{T}\right)\frac{d\hat{U}_s}{dx}. \tag{34}$$

with $\Phi_0 = \mu\alpha$, $\mu = \sqrt{3/S_{q0}B_0}$ and $La = (w_*/U_S(0))^{1/2}$ is the turbulent Langmuir number. Here, the left-hand side of the dimensionless form of the TKE equation contains the processes which are usually encountered in the atmospheric surface layer, namely diffusion, dissipation, turbulence production by shear and buoyancy. The stability parameter ζ is defined as $\zeta = z/L$ where L is the Obukhov length scale

$$L = \frac{\rho w_*^3}{\kappa g \nu_h d\rho/dz}. \tag{35}$$

which is the height where shear production and buoyance balance. Making use of the temperature profile and the relation between density gradient and temperature gradient, the Obukhov length becomes

$$L = \frac{\rho_w c_p w_*^3}{\kappa g \alpha_w \left(Q_h + R(0) - R(z)\right)}. \tag{36}$$

and, because of the local definition of the Obukhov length, radiative forcing is included in a natural way in the expression for L (cf. Large *et al.*, 1994). The right-hand side of (33) gives the effects of ocean waves on the mixing in the upper ocean: the first term represents effects of wave dissipation which affect mixing close to the ocean surface, while the second term (which depends on the turbulent Langmuir number) represents the effect of Langmuir circulation which transports heat and momentum to the deeper parts of the ocean.

The differential equation for w, Eq. (33), has of course to be supplemented by boundary conditions. They are given in Eqns. (24)-(25). In terms of the unknown w they become

$$\frac{dw}{dx} \to 0 \text{ for } x \to -\infty;\ w \to 1 \text{ for } x \to \infty, \tag{37}$$

4.1 The Local Approximation.

It is, as far as I know, not possible to obtain for the general case the exact solution of the nonlinear boundary value problem (33), (37). Therefore, an approximate solution is obtained by showing that in the present context effects of diffusion can be ignored and the search for the turbulent velocity reduces then to solving an algebraic equation. Note that this approach is not feasible in the original Graig-Banner problem because diffusion is essential in order to transport the turbulent kinetic energy through the surface layer. However, here a different route is followed as the pressure vertical velocity correlation term in the TKE equation has been explicitely modelled in terms of the energy flux and the profile function $\hat{T}$.

Let us now study the solution of the boundary value problem (33), (37). It should be noted that (33) is a nonlinear differential equation which only in cases where a first integral can be found may be solved exactly. An example is given in Janssen *et al.* (2004) who solved the Craig-Banner problem exactly. However, when effects of buoyancy are present or when Langmuir turbulence and wave dissipation (in the form modelled here) is important it is not possible to find a first integral. Therefore an alternative approach will be followed which was suggested by Øyvind Saetra. In fact, this approach was also followed by Craig (1996) although it is not mentioned explicitely in his paper. Inspecting the differential equation for w it is realized that the nonlinearity only comes from the $w^{-1/3}$ term and therefore the nonlinearity is fairly weak. It is therefore suggested to replace the $w^{-1/3}$ term by its equilibrium value for large x. Far away from the sea surface the diffusion term vanishes while also the wave dissipation and Langmuir circulation term $S(x)$ becomes small. However, it is not known how the buoyancy terms behaves for large x so in the present discussion effects of buoyancy are ignored. The equilibrium value for w then follows from the balance of shear production and dissipation (which is the 'typical' situation in the atmospheric surface layer), hence $w = (1-\hat{T})^{3/2}$. Therefore, the nonlinear differential equation for w becomes approximately

$$\frac{d^2w}{dx^2} - w = -(1-\hat{T}(x))^{3/2} + S(x) \tag{38}$$

It is straightforward to solve the linear boundary value (37)-(38) by means of the Green function technique. The solution becomes

$$w = \int_{-\infty}^{\infty} \mathrm{d}x_0 \, G(x,x_0) \left[-(1-\hat{T}(x_0))^{3/2} + S(x_0) \right]. \tag{39}$$

where the Green function $G(x,x_0)$ is given by

$$G(x,x_0) = \begin{cases} -\frac{1}{2} e^{x-x_0}, & x < x_0, \\ -\frac{1}{2} e^{x_0-x}, & x > x_0. \end{cases} \tag{40}$$

The current profile can easily be obtained by rewriting Eq. (13) in terms of an integration over the x-variable. The result is

$$u(z)/w_* = -\tau_0^{1/2} \int_{x_h}^{x} \frac{\mathrm{d}x}{w^{1/3}} \left(1-\hat{T}\right), \tag{41}$$

where $\tau_0^{1/2} = (S_{q0}B_0/3)^{1/2}$ and where $x = x_h$ corresponds to the depth H where the current profile vanishes. In this Section $H = 5H_S$ is chosen.

The solution (39-41) is readily evaluated on the computer. In order to do this the decay length scale z_0 of the wave-induced stress needs to be specified, i.e.

$$z_0 = 0.5 H_S, \tag{42}$$

and H_S is the significant wave height, $H_S = 4m_0^{1/2}$, with m_0 the zeroth moment of the wave spectrum. The windspeed is 2.5 m/s, the turbulent Langmuir number is 1/4 and the dimensionless energy flux α is equal to 100, which is a typical value in the Tropics (see Fig. 3). This low wind speed example has been chosen because under these circumstances a diurnal cycle in the sea surface temperature and in the surface drift may be present. In this example it is assumed that there is only windsea present, so the significant wave height follows from $H_S = \beta U_{10}^2/g$, with $\beta = 0.22$. The Stokes drift decay length scale then follows from $k_s = g/U_{10}^2$. For U_{10}= 2.5 m/s the significant wave height is only 14 cm so that the 'roughness' length is about 7 cm. The air friction velocity u_* is 8 cm while the water friction velocity w_* is about 0.3 cm. Finally, the Stokes wavenumber k_s is about 1.6 rad/m.

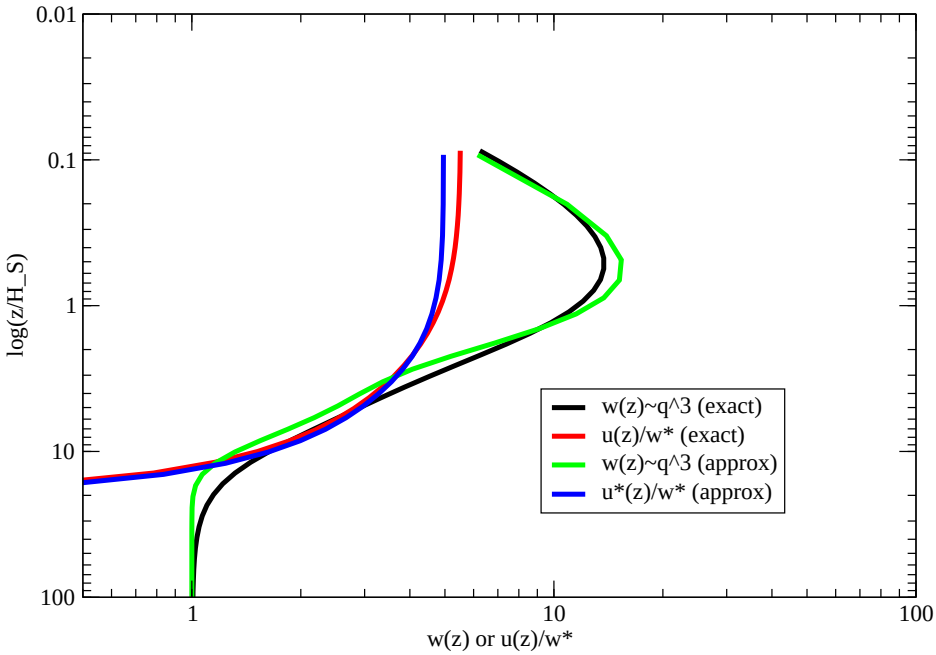

Figure 4: Profile of $w = Q^3$ and current profile in the ocean column near the surface. The approximate solution (43), based on the slowly varying wave dissipation source function and the gradient in the Stokes drift, are shown as well.

Results for w and current $u(z)/w_*$ as function of dimensionless depth z/H_S are displayed in Fig. 4. Note that there are important differences between this solution and the results of Graig and Banner (1994). While in their approach w obtains its maximum value at the surface $z = 0$, this is evidently not the case in the present approach as the maximum is now at about a depth of the order of the significant wave height (which makes by the way perfect sense).

The solution (39) although elegant is still awkward to deal with in practical applications because an integral needs to be evaluated. However, the Green's function (40) looks like a δ-function, therefore assuming that the bracket term in (39) varies slowly compared to the Green's function one finds the approximate solution

$$w \approx (1 - \hat{T}(x))^{3/2} - S(x), \tag{43}$$

and the approximate solution for $w(z)$ and $u(z)/w_*$ is shown in Fig. 4 as well. The agreement between approximate and exact solution seems fair. Note that the approximate solution, which from now on will be referred to as the *local approximation*, is based on the assumption that the production and dissipation terms are slowly varying with respect to the diffusion. In fact, (43) follows immediately from the neglect of the turbulent diffusion term in the kinetic energy budget (33).

In terms of the depth variable z the solution (43) can be written explicitely as

$$w \approx (1 - \hat{T})^{3/2} - \alpha\kappa z f_M \frac{d\hat{I}_w}{dz} - La^{-2}\kappa z f_M (1 - \hat{T}) \frac{d\hat{U}_S}{dz}, \tag{44}$$

and it is now straightforward to estimate the respective contributions of shear production, wave dissipation and Langmuir turbulence to the dimensionless turbulent velocity $Q = w^{1/3}$. This will be done by taking the maximum of the individual terms. The maximum of the shear production term is 1, while the maximum of the

wave dissipation contribution is $\alpha\kappa e^{-1} \approx 15$ at $z = z_0$ and the maximum contribution by Langmuir turbulence is $La^{-2}\kappa e^{-1} \approx 2$ (at $z = 1/2k_s$). Based on these estimates it seems that near the surface the most relevant process for mixing is wave dissipation because it is an order of magnitude bigger than the other two terms, however the turbulent velocity is only enhanced by a factor 2.5 because the sum of the contributions is raised to the power 1/3. Nevertheless, Langmuir turbulence should be relevant as well as this process penetrates into the deeper layers of the ocean. This is illustrated in Fig. 5 for the special case of low wind of this §. For comparison

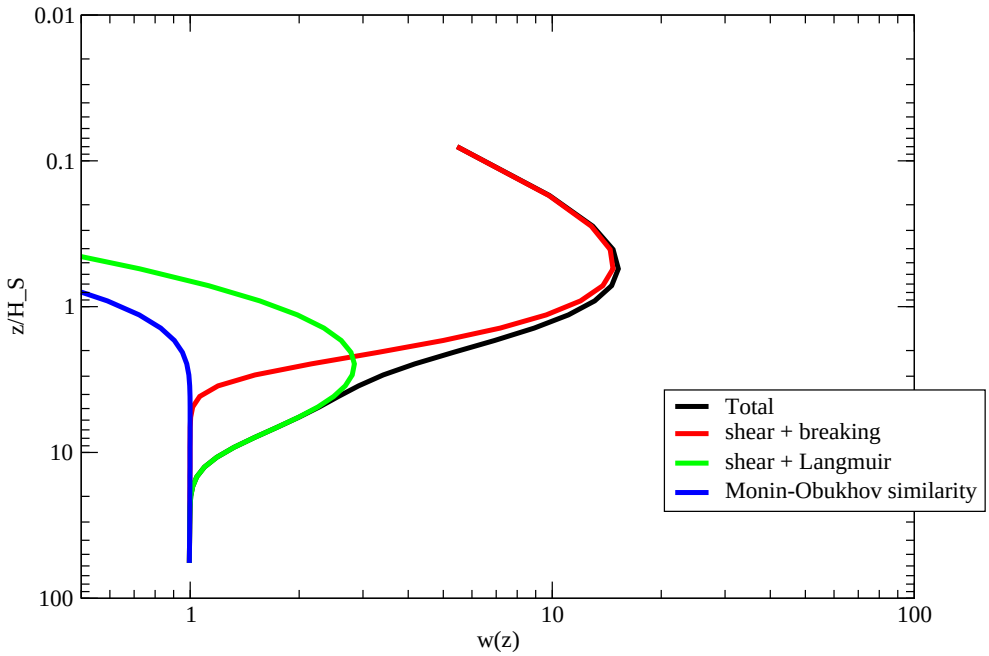

Figure 5: Profile of $w = Q^3$ according to the local approximation in the ocean column near the surface. The contributions by wave dissipation (red line) and Langmuir turbulence (green line) are shown as well. Finally, the w-profile according to Monin-Obukhov similarity, which is basically the balance between shear production and dissipation, is shown as the blue line.

purposes I have shown the *w*-profile in case of Monin-Obukhov similarity, which consists of a balance between shear production and dissipation, and I have shown the impact of switching off Langmuir turbulence and wave dissipation. The Figure shows that indeed the maximum in *w* by wave dissipation is close to the sea surface at a depth $z = z_0$ while the maximum by Langmuir turbulence is at larger depth of $1/2k_s$. These scales are widely different because ocean waves are weakly nonlinear which means that their 'typical' steepness $k_s H_S << 1$. As a consequence the ratio of the penetration depths by wave dissipation and Langmuir turbulence, given by $2k_s z_0 = k_s H_S$, is small as well.

Therefore it is evident that there are two regimes. The first one is close to the surface and is dominated by wave dissipation. Around 4 times the roughness length a transition to a different regime is to be noted, namely one dominated by the production of Langmuir turbulence. Hence, it is seen that there are two transport mechanisms operating in the surface layer of the ocean. Up to a few wave heights wave dissipation is dominant in the diffusion of momentum and heat and the transport of these quantities is taken over by Langmuir turbulence in the deeper part of the surface layer. The enhanced transport by wave processes gives rise to much flatter profiles near the surface. This may be inferred from Fig. 6 where current profiles from the Monin-Obukhov similarity model are compared with current profiles when wave dissipation and Langmuir turbulence play a role. The

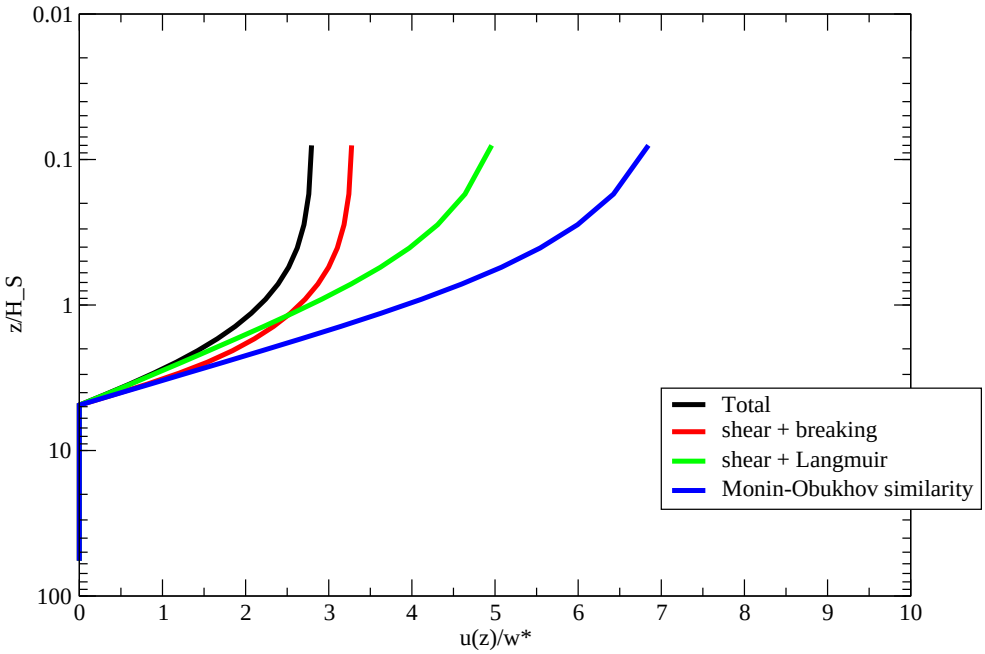

Figure 6: Current profile near the surface. The impact of wave dissipation and Langmuir turbulence is shown as well. The Monin-Obukhov similarity gives the usual logarithmic profile.

surface current reduces from about[3] $7w_*$ to $2.5w_*$, which is a considerable reduction. As a consequence, it is expected that these two processes will play an important role in the determination of the amplitude of the diurnal cycle. Finally, it is also concluded that a mixed layer model which has only a representation of Langmuir turbulence is not sufficient as it will overestimate the amplitude of the diurnal cycle. If one is interested in modelling the diurnal cycle then probably only the first few metres of the upper ocean need to be considered. In that event wave dissipation is seen to be the dominant process for heat transport, however there is no reason to disregard effects of Langmuir turbulence from the outset as it is very straightforward to take both into account. In addition, during the duirnal cycle there will also be episodes when the flow is neutrally stable or unstable. Langmuir turbulence will then play a pronounced role.

This Section is concluded with the following comment. So far two things have been learned. First, if one describes the effect of wave dissipation through the correlation term of pressure and vertical velocity it seems a valid assumption to neglect the effects of the diffusion of turbulent kinetic energy. Second, it seems possible to combine in a simple way several physical processes that affect the mixing in the upper-ocean. From the previous discussion it appears that if one has, apart from shear production S_P, several processes $P_1, P_2, P_2, \ldots$ that contribute to turbulent mixing then the turbulent velocity $q(z)$ of the combination of all those processes is, following Eq. (43), given by

$$q = \left\{ S_P^{3/4} + P_1 + P_2 + P_3 + \ldots \right\}^{1/3}.$$

The reason that processes can be added via an '1/3'- rule is because dissipation is proportional to the third power of q, while the shear production term has been linearized by replacing $w^{1/3}$ by its equilibrium value and

[3] Using the approximate solution given in the Remark on page 10 one may estimate the surface current in case of Monin-Obukhov similarity. One finds $u(0)/w_* \approx log(H/y_0)/\kappa = 7.23$, with $H = 5H_S$. Using a higher resolution version of my software a perfect match with the approximate result is found.

the other processes are assumed to be independent of the turbulent velocity q. Because of the '1/3'- rule it makes sense, as done in the present work, to make plots involving $w = Q^3$ as for w different processes may be added.

The '1/3'- rule also gives rise to consistent scaling behaviour in case of Monin Obukhov similarity. This is the case that there is no wave dissipation and no generation of Langmuir turbulence. In that event, w from Eq. (43) becomes $w = (1-\hat{T})^{3/2}$ and the current profile becomes (cf Eq. (41)

$$u_0(z) = -\tau^{1/2} \int_{x_h}^{x} \frac{\mathrm{d}x}{w^{1/3}} \left(1-\hat{T}\right)^{1/2}$$

therefore the current scales with the square root of $1-\hat{T}$ which agrees with the scaling behaviour mentioned in the Remark on page 10. Nevertheless, it should be pointed out that the '1/3'- rule is not always appropriate. In particular, the buoyancy term has so far not been considered but this effect is expected to play an important role far away from the surface, thus making it difficult to give an estimate of the equilibrium value of q. In addition, the buoyancy term is a fairly sensitive function of q and therefore it is not easy to linearize it.

In the remainder of this Section I will therefore refrain from linearizing the shear production term, but I will disregard the effect of diffusion of turbulent kinetic energy. Therefore, the TKE equation becomes, neglecting diffusion in (23),

$$\frac{\partial e}{\partial t} = \frac{\partial I_w(z)}{\partial z} + \nu_m S^2 - w_*^2 \frac{\partial U_S}{\partial z} - \nu_h N^2 - \frac{2\sqrt{2}}{Bl(z)} e^{3/2}. \tag{45}$$

and in terms of the dimensionless variables introduced in this Section one has, with dimensionless time $\tau = S_M^2 w_* t/l(z)$,

$$\frac{1}{2}\frac{\partial}{\partial \tau} Q^2 = -\frac{1}{Q}\left(Q^4 - \alpha(Q)Q - \beta\right), \tag{46}$$

where

$$\alpha(Q) = -\zeta f_M - S(x),\ \beta = \left(1-\hat{T}\right)^2.$$

and α still depends on Q through the buoyancy term $-\zeta f_M(Ri_t)$. For completeness the source function, which represents effects of wave dissipation and Langmuir turbulence, is repeated from Eq. (34):

$$S(x) = \Phi_0 \frac{d\hat{I}_w}{dx} + \mu La^{-2}\left(1-\hat{T}\right)\frac{d\hat{U}_s}{dx}.$$

In the local approximation the TKE equation has now been simplified considerably, and the search for its equilibrium solution has been reduced to the solution of an almost quartic problem. For example, for the neutrally stable case the equilibrium solution to Eq. (46) follows from the real, positive root of the quartic equation $Q^4 - \alpha Q - \beta = 0$ and it can readily be shown that the '1/3'-rule is a good approximation to this root. In the next section (46) is used in a discussion on stratification effects.

4.2 Effects of stratification.

First, effects of stratification in the atmospheric context will be studied and the findings will be applied to the mixed layer of the upper ocean. In the atmosphere close to the surface there is a balance between shear production, buoyancy and dissipation, as forcing is usually absent. This will be called the case of Monin-Obukhov similarity.

4.2.1 *Monin-Obukhov similarity.*

In the atmosphere, stability effects are usually studied in terms of the dimensionless shear function ϕ_m and the dimensionless virtual potential temperature gradient ϕ_h. These dimensionless functions are defined as

$$\phi_m = \frac{\kappa z}{u_*}\left|\frac{\partial u}{\partial z}\right|, \;\; \phi_h = \frac{\kappa z}{\theta_*}\frac{\partial \theta_v}{\partial z}, \tag{47}$$

where u_* is the air friction velocity and $\theta_* = -\overline{w'\theta'_v}/u_*$ is a turbulent temperature scale. The dimensionless shear function measures deviations from neutral circumstances as for the logarithmic wind profile $\phi_m = 1$, and similarly ϕ_h measures deviations from the logarithmic virtual temperature profile. Using the local scaling theory of Nieuwstadt (1984) it can be argued that the profile functions are only a function of the stability parameter $\zeta = z/L$, where L is the local Obukhov length defined as

$$L = -\frac{u_*^3\theta_v}{\kappa g \Phi_h} \tag{48}$$

Here θ_v is the virtual potential temperature and $\Phi_h = \overline{\delta w \delta \theta_v}$ is the virtual potential temperature flux. The shape of the ϕ functions is usually determined from observations acquired during field campaigns, but high measurement accuracy is required because the fluxes become weak during strongly stable conditions. Alternatively, a realistic theoretical model of turbulent flows with stable stratification has been developed by Sukoriansky *et al.* (2005) providing additional information on how to model stratification effects.

The Kansas field campaign (Businger *et al.*, 1971)[4] was one of the first experiments to propose realistic parametrizations for the ϕ functions. For stable conditions it was found that ϕ_m and ϕ_h varies essentially linearly with ζ over the observed stability range between 0 and 1. A fit gives

$$\phi_m = 1 + 4.7\zeta, \; \phi_h = 0.74 + 4.7\zeta, \;\; \text{for} \;\; 0 < \zeta < 1. \tag{49}$$

On the other hand, for unstable conditions a good fit was found to be

$$\phi_m = (1 - 15\zeta)^{-1/4}, \;\; -2 < \zeta < 0. \tag{50}$$

A similarly looking fit was found for ϕ_h. However, in the upper ocean strongly stable conditions occur with ζ of the order 10 or even larger. These conditions are much more extreme than typically encountered for the atmospheric surface layer except perhaps for air flow over ice. Therefore, relatively little is known in these extreme circumstances, and in fact conflicting conclusions about properties of strongly stable turbulence have been reached in the past. The problem is best illustrated by the behaviour of the Prandtl number Pr defined as

$$Pr = \frac{\nu_m}{\nu_h} = \frac{\phi_h}{\phi_m},$$

as function of the gradient Richardson number Ri given by

$$Ri = \frac{N^2}{S^2}.$$

A vast number of studies (see e.g. Kondo *et al.*, (1978); Kim and Mahrt (1992), Strang and Fernando (2001), Sukoriansky *et al.* (2005), Zilitinkevich *et al.* (2007) and many others) suggest that for strongly stable flow, hence for a Richardson number larger than the critical value of 1/4, the Prandtl number is larger than 1, while

[4] Note that in order that $\phi_m(\zeta = 0) = 1$ the authors had to choose a von Kármán constant of 0.35, which does not agree with the accepted value of 0.4.

for small Ri (the neutral limit) the Prandtl number is smaller than 1 (as is evident from Eq. (49)). In other words, for strongly stable flow, momentum is mixed more efficiently than heat. This is thought to be an indication of internal gravity wave activity which can produce transfer of momentum but only little heat transfer (as long as the waves do not break).

However, in sharp contrast to these findings, Cheng and Brutsaert (2005) and Grachev *et al.* (2007) conclude from the SHEBA observations, which were obtained for strongly stable flow over ice, that heat transport is more efficient than momentum transport hence $Pr < 1$. Grachev *et al.* (2007b) have analyzed their findings in some detail, but no physical explanation has been offered. They point out that there is a spurious correlation between $Pr = \phi_h/\phi_m = Ri/Ri_f$ and measures of stability such as the local Richardson number $Ri = \zeta\phi_h/\phi_m^2$, the flux Richardson number $Ri_f = \zeta/\phi_m$ and the stability parameter $\zeta = z/L$ because Pr and these stability parameters share parameters such as vertical gradients in mean wind speed and potential temperature and the corresponding fluxes. But the argument of spurious correlation is not really convincing, as theoretical developments such as given by Sukoriansky *et al.* (2005), who applied renormalization techniques to find the Richardson number dependence of eddy viscosity ν_m and eddy diffusitivity ν_h, show that $Pr > 1$ for large Ri. Also direct numerical simulation results by Shih *et al.* (2000) and the observations of Strang and Fernando (2001) confirm this.

Furthermore, both Cheng and Brutsaert (2005) and Grachev *et al.* (2007) find a levelling-off of the similarity functions ϕ_m and ϕ_h as a function of the stability parameter ζ which is so large that it conflicts with the steady state TKE equation. In order to see this, apply now the TKE equation (46) to the atmospheric problem where forcing is absent. In the steady state one then finds

$$Q^4 + \zeta f_M Q - 1 = 0. \tag{51}$$

The similarity functions can be written in terms of the present dimensionless variables and the result is

$$\phi_m = \frac{1}{Q f_M}; \;\; \phi_h = \frac{1}{Q f_H} \tag{52}$$

Expressing Q in terms of ϕ_m and substituting the result into (51) gives

$$\phi_m^4 - \zeta\phi_m^3 - f_M^{-4} = 0. \tag{53}$$

For neutrally stable conditions, Eq. (53) reduces to the well-known KEYPS formula $\phi_m^4 - \zeta\phi_m^3 - 1 = 0$ (Panofsky, 1963). This is usually regarded as an equation for the dimensionless shear function. It is advantageous, however, to turn things around, i.e. to regard (53) as an equation for f_M because ϕ_m is known from the observations. Rearranging (53) one finds for f_M

$$f_M = \left[\phi_m^3(\phi_m - \zeta)\right]^{-1/4}. \tag{54}$$

From (54) it immediately evident that there is only a real solution for f_M when $\phi_m > \zeta$. If the TKE equation (53) holds then the condition $\phi_m > \zeta$ has important implications for parametrizations of the dimensionless shear function. For example, the Grachev *et al.* (2007) parametrization for ϕ_m becomes according to (54) unrealistic because it will cross the line $\phi_m = \zeta$ for $\zeta \approx 17$, which is well inside the stability range that the dimensionless shear has been observed. This result can also be understood in physical terms. The present TKE equation expresses a balance between shear production, buoyancy and dissipation. Now dissipation is always positive therefore buoyancy can never exceed production, or in terms of the present dimensionless variables, $\phi_m > \zeta$. Clearly, in the context of the present TKE formulation it is not possible to model a levelling off of the dimensionless shear function as found in the SHEBA data set by Grachev *et al.* (2007a) and by Cheng and Brutsaert (2005). A possible resolution of the conflict between the SHEBA data set (strongly stable flow over ice) and the standard TKE equation, which is based on a balance between shear production, buoyancy and

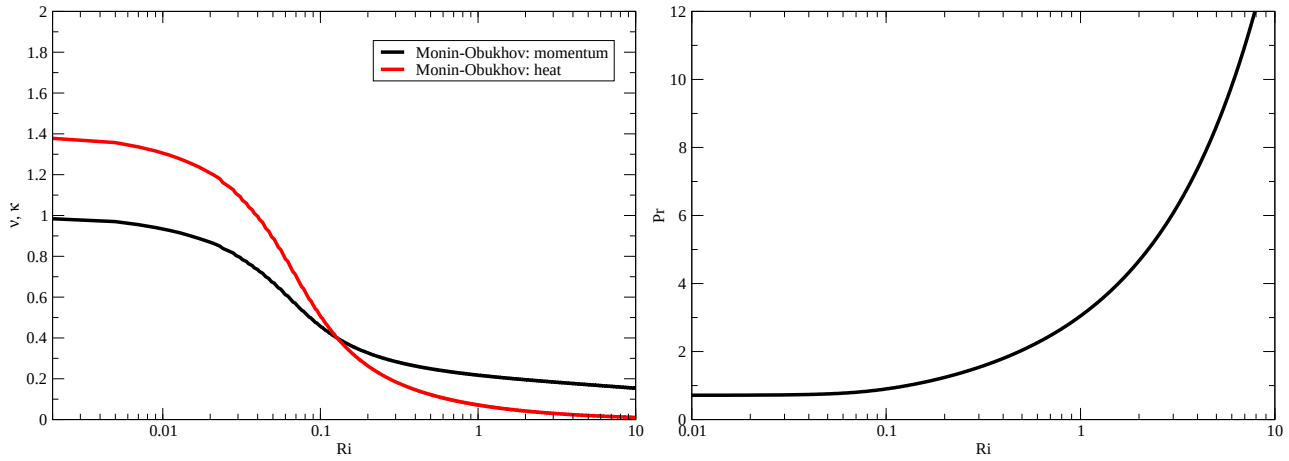

Figure 7: Eddy viscosity ν_m and heat diffusivity ν_h as function of the local Richardson number Ri. In the right panel the Prandtl number Pr is shown as function of Ri.

dissipation, might be that during SHEBA there was an additional source for the production of turbulent kinetic energy. Thus, the SHEBA results cannot be used as a guideline for the present modelling work.

In order to be specific a choice has to be made for the coefficients in the parametrization (30) of f_M and f_H. This choice will be based on the one hand on the Kansas field results in the weakly stable limit, while for the strongly stable limit guidance from the renormalization work of Sukoriansky *et al.* (2005) is taken. In particular, the following choice for f_M and f_H is made:

$$f_M = a_M(1+b_M Ri_t)^{-1/2} + c_M, \quad f_H = a_H(1+b_H Ri_t)^{-1/2} \tag{55}$$

where $a_M = 0.8$, $b_M = 100$, $c_M = 0.2$, $a_H = 1.4$ and $b_H = 80$. From (55) it is seen that f_H vanishes for large Ri_t while f_M asymptotes to a finite value of $c_M = 0.2$. For small turbulent Richardson numbers f_H is larger than f_M, hence, with $Pr = \phi_h/\phi_m = f_M/f_H$, it is found that $Pr \approx 0.71 < 1$ for $Ri_t \to 0$ in agreement with results from the Kansas field campaign. In order to determine some of the coefficients an approximate solution was used. In fact, an approximate solution for the dimensionless turbulent velocity Q may be found for small values of the stability parameter ζ. One finds $Ri \approx \zeta/a_H$ and the eventual result for the dimensionless shear function is

$$\phi_m \approx 1 + \frac{1}{4}\zeta\left[1 + 2(1-c_M)b_M S_0^2/a_H\right].$$

but this approximation is only valid for a relatively small range of the stability parameter, $\zeta < 0.1$. The choice of coefficients given below Eq. (55) together with $S_0 = .39$ gives a value of the slope of 4.6 which is close to the value reported by the Kansas field campaign given in Eq. (49). In addition, anticipating results discussed below the right panel of Fig. 7 shows that up to a gradient Richardson number of 0.1 the Prandtl number is a constant so that in agreement with the Kansas data ϕ_h has the same slope as ϕ_m for small ζ.

On the other hand, for large turbulent Richardson number, $Ri > 0.2$, the Prandtl number is larger than 1, indicating that in this domain momentum transfer is more efficient than heat transport, in agreement with Sukoriansky *et al.* (2005) and the observations of Strang and Fernando (2001). In order to show explicitely the effect of buoyancy on the transport properties, the eddy viscosity ν_m and heat diffusivity ν_h are normalized with the eddy viscosity $\nu = \kappa u_* z$ for neutrally stable flow. In terms of the present dimensionless variables one finds $\nu_m/\nu = f_M Q$ while $\nu_h/\nu = f_h Q$, hence the normalized viscosities are simply the inverse of ϕ_m and ϕ_h. Using (55) in (51) and solving for Q by iteration the resulting transport coefficients as function of the Richardson number $Ri = \zeta\phi_h/\phi_m^2$ are shown in the left panel of Fig. 7, while the Prandtl number Pr as function of Ri is shown in the right panel. Comparing this Figure with Figs. 8 and 9 of Sukoriansky *et al.* (2005) it is seen that

there is good qualitative agreement with the results using renormalisation techniques to obtain the transport coefficients. In particular, as already pointed out, a finite value of c_M in (55) does not give rise to a critical value of the gradient Richardson number as a finite c_M represents additional diffusion by e.g. internal gravity waves and/or intermittency. At the same time, the consequence is that for large Richardson number momentum transport dominates heat transport.

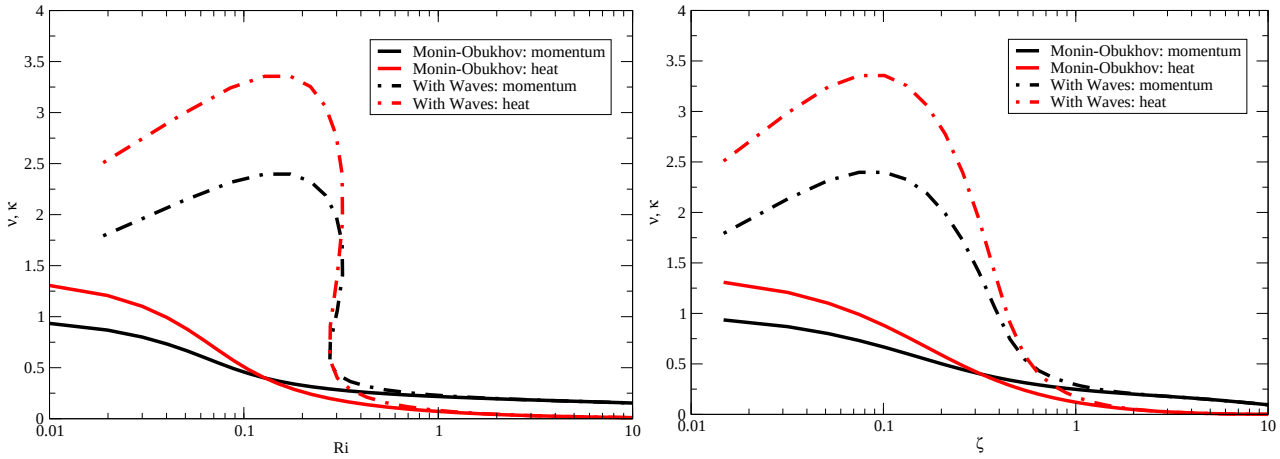

Figure 8: Eddy viscosity ν_m and heat diffusivity ν_h as function of the local Richardson number Ri, showing the effects of wave dissipation and Langmuir turbulence. In the right panel the same parameters are shown as function of the stability parameter ζ.

4.2.2 Wave effects and buoyancy.

In this section the combined effects of wave dissipation, Langmuir turbulence and buoyancy on the properties of turbulence in the mixed layer are studied. It is assumed that the parametrization of stratification for the atmosphere (cf Eq. (55)) also holds for the oceanic case. The set of equations to be solved consists of the steady state version of (46) together with (28), (30), and (36). This set of equations does not have an exact solution because owing to effects of stability α in (46) depends strongly on the dimensionless turbulent velocity Q. The set of equations was therefore solved by means of an iteration scheme using starting values $Q = 1$, $f_M = f_H = 1$. Because the stability effects are modelled in terms of the turbulent Richardson number $Ri_t = Nl(z)/q$, the Brunt-Väisälä frequency needs to be expressed in terms of Q. Introducing $N_* = l(z)N/w_*$ one finds $N_*^2 = \zeta / f_H Q$.

In Fig. 8 effects of wave dissipation and Langmuir turbulence on transport coefficients for momentum and heat is shown. In the left panel these coefficients are plotted as function of the gradient Richardson number Ri, while in the right panel they are shown as function of the stability parameter ζ. Of course, waves gives rise to enhanced transport, but, remarkably, in the presence of this additional forcing the transport coefficients are not a single-valued function of Ri. However, in terms of the turbulent Richardson number Ri_t or the stability parameter ζ (as shown in the right panel of Fig. 8) the transport coefficients are unique functions.

In Fig. 9 effects of stratification on the profile for $w = Q^3$ as function of dimensionless depth z/H_S are shown. For this plot the parameters from the example in §4.1 are used and, in addition, the heat flux Q_h was 100 W/m^2 while the water temperature T was 303 K. In order to vary the Obukhov length scale L, as determined by Eq. (36), wind speed values of 2.5, 1.25 and 1 m/s were used respectively. It is instructive to compare results for $w(z)$ with the case of no stratification. It is then immediately seen that, as expected, buoyancy has the biggest impact on the turbulent velocity Q in the deeper layers of the ocean (note that $L = 0.76$ corresponds to

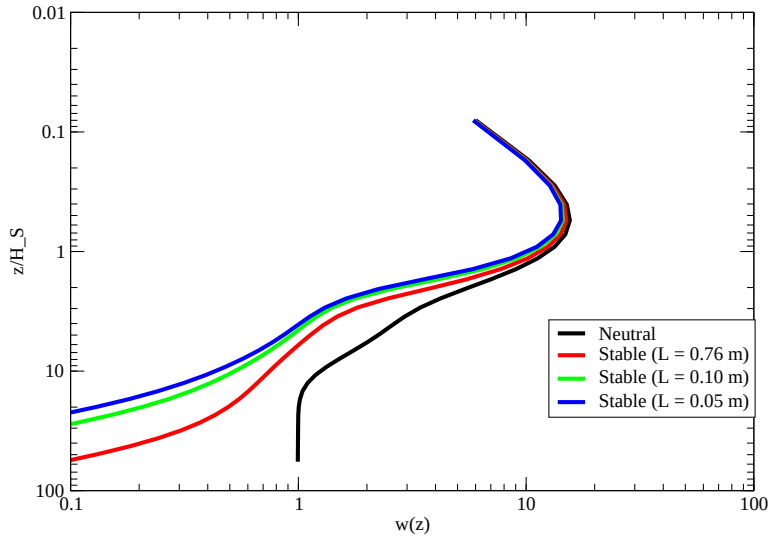

Figure 9: Dependence of $w(z)$-profile on effects of buoyancy.

$L \approx 5H_S$). This means that according to this model the impact of Langmuir turbulence on upper ocean mixing is considerably reduced in stable circumstances. For these particular examples the maximum in w, caused by wave dissipation, is hardly affected by stability effects. Surpringly perhaps, this is a fairly general result. Only when the heat flux was increased by a factor of 10 an appreciable reduction of the impact of wave dissipation on the mixing was found (not shown). This apparent robustness of the wave dissipation impact on mixing can be understood by once more noting that the maximum of $w(z)$ occurs at $z = z_0$, where according to the present model the roughness length scales with the square of the friction velocity. A significant impact of buoyancy on the maximum is expected when $L \leq z_0$. Using the definitions for L and z_0 one finds $U_{10} \leq 3 \times 10^{-4} Q_h$ which, even with a large value of Q_h of 1000 W/m^2, is still a small wind speed.

Finally, in Fig. 10 the impact of stability on the equilibrium current is shown. The increase of the surface current for increasing stability is mainly caused by the reduction of the effects of Langmuir turbulence. The Figure illustrates that also in the surface current a diurnal cycle is to be expected. As a general remark it is noted that under unsteady circumstances the impact of effects of stability, wave dissipation and Langmuir circulation is somewhat reduced, while the temperature and current profile may occasionally be convex rather then concave as in the steady state case. This will be shown in more detail in the next Section during a discussion of the simulation of the diurnal cycle in SST.

4.2.3 A qualitative validation.

The present experimental knowledge of turbulence in the ocean surface layer is summarized by the works of Terray *et al.* (1996), Drennan *et al.* (1996) and Anis and Moun (1995). Here, dimensionless dissipation, defined as $\varepsilon_* = \varepsilon H_S / F_0$ with F_0 the energy flux into the ocean, is found to be a function of dimensionless depth $(z+z_0)/H_S$. In the case of Monin-Obukhov similarity one would expect that the 'Law of the Wall' holds which states that dissipation scales with z^{-1} as the turbulent velocity is constant. However, according to observations of turbulence near the surface dissipation depends in a more sensitive manner on depth. Based on work Terray *et al.* (1999) and of Burchard (2001), who summarised the observational knowledge, one finds near the surface

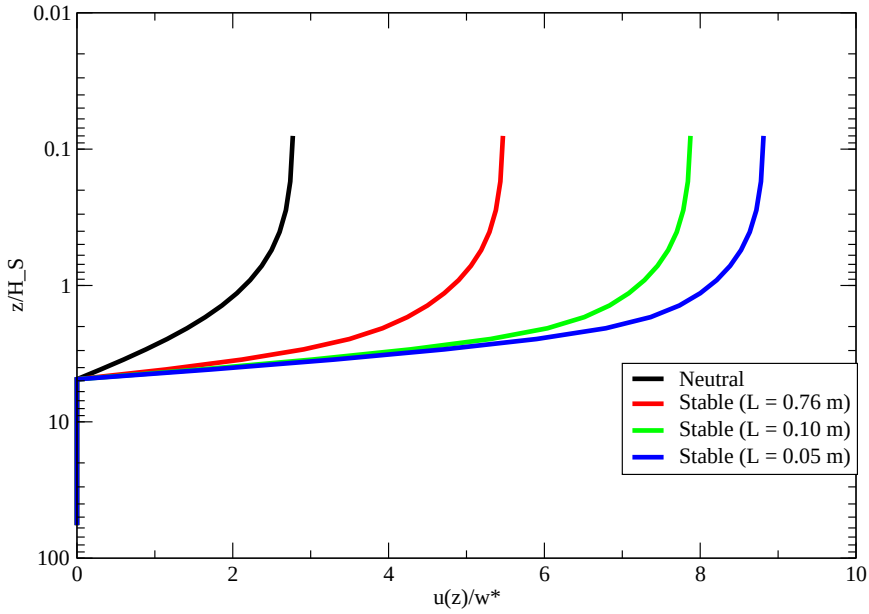

Figure 10: Dependence of near-surface current profile on effects of buoyancy.

the fit

$$\varepsilon_* = 0.78 Z^{-2.78}, \quad Z = (z + z_0)/H_S.$$

which is valid for $\varepsilon_* > 0.01$. These observations are quite useful to determine an important parameter in the mixed layer scheme, namely the roughness length z_0 or the corresponding gradient length scale of the wave dissipation source function. Burkhard finds an optimal fit (however using a somewhat different turbulence model) when $z_0 = 0.5 H_S$. This finding has been confirmed here. In order to illustrate that the present model indeed gives the correct scaling behaviour, Fig. 11 shows dimensionless dissipation versus $(z + z_0)/H_S$ for the strongly stable case and for neutral stability and compares the model results with the above power law. The agreement between the neutrally stable case and the fit to the data seems fair. Also note that according to the present mixed-layer model there is a transition from wave dissipation driven turbulence to shear driven turbulence, giving the 'Law of the Wall' in the deeper layers of the ocean, while in the transition layer turbulence is controlled by production of Langmuir circulation.

5 Numerical simulation of the diurnal cycle in SST and surface current.

In this section the mixed layer model described in §3 is applied to a simulation of the diurnal cycle in sea surface temperature (SST) and the surface current. The relevant equations are (11), (12), (14), (15) and (23). The boundary condition for the momentum equation is vanishing turbulent stress at the surface, while for the temperature equation the turbulent heat flux at the surface is given by $Q_h/(\rho_w c_p)$. The turbulent kinetic energy flux at the surface vanishes as well. At depth $z = D$, where in the present application D is of the order of 3 m, current velocity $u(z)$ and temperature $T(z)$ are assumed to be given.

The equations for momentum, heat and turbulent kinetic energy are discretized in the vertical in such a way that the fluxes are conserved, while the relevant quantities are advanced in time using an explicit scheme. The

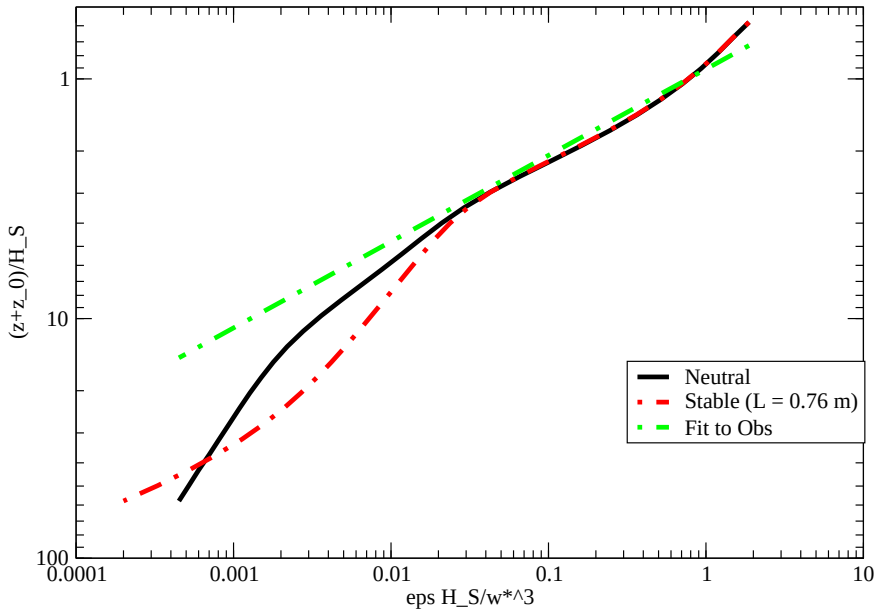

Figure 11: Dimensionless dissipation $\varepsilon_* = \varepsilon H_S/F_0$ versus $(z+z_0)/H_S$

time step was chosen to be 2 seconds and in order to garantee stability a limitation on the size of the diffusion coefficients was imposed. With n labelling a particular layer and N the total number of layers, the vertical discretization is obtained using a logarithmic transformation of the type

$$z(n) = z_s\left(e^{\xi(n)} - 1\right), \quad n \leq N,$$

where $\xi(n) = n\Delta$ is discretized in a uniform manner and $\Delta = \log(D/z_s + 1)/N$. Typically, z_s is of the order of a few centimetres thus giving high resolution near the surface, which is needed to resolve the solar absorption profile (15) appropriately, while away from the surface resolution degrades. For the simple example of constant wind and sea state discussed below z_s is chosen to be one-third of the roughness length z_0 as it can be easily shown that the mixing scales with z/z_0. In that case depth D becomes a multiple of the roughness length, $D \approx 110 z_0$. However, in the general case of varying winds the transformation for $z(n)$ would become time-dependent. Although it is straight-forward to deal with a time-dependent coordinate transformation, it was decided to choose for the general case a constant z_s with $z_s = 0.025$ m. Then the depth D is a constant as well, $D = 3.5$ m as observations of temperature at that depth are available. In all applications the number of layers N is equal to 8.

Finally, when integrating the TKE equation forward in time numerical errors may introduce small negative turbulent kinetic energy so that determination of the turbulent velocity would fail because of taking the square root of the energy. For security reasons, therefore, a minimum value of turbulent kinetic energy is introduced being a small fraction of the equilibrium turbulent kinetic energy, $e_{min} = 0.0001 w_*^2/2$.

5.1 Synthetic example.

As a first test a five day simulation was performed with constant fluxes of momentum τ and heat flux Q while the solar radiation followed a daily cycle according to $R = R_0 \max[\sin(\omega t), 0]$ where $\omega = 2\pi/(24 \times 3600)$. The intention is to generate a steady daily oscillation in SST without drift in the temperature and to study effects

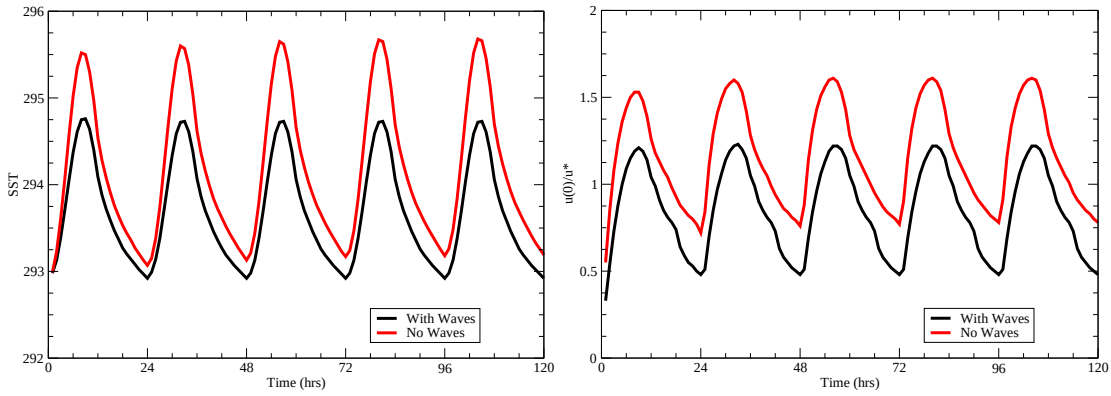

Figure 12: The left panel shows for pure windsea time series of SST for a constant wind speed of 2.5 m/s and a heat flux of -150 W/m^2, while the daily average solar insolation is 350 W/m^2. The impact of disregarding ocean wave effects is shown as well. The right panel shows the surface current normalized with the air friction velocity.

of ocean waves on shape and amplitude of the daily cycle. In order to achieve a steady oscillation values of daily average insolation, heat and momentum flux have to be chosen appropriately. The momentum flux τ was chosen equal to 0.0069 m^2/s^2, which, with a drag coefficient of 1.11×10^{-3}, corresponds to a wind speed of 2.5 m/s, while the heatflux was given the value - 150 W/m^2 typical for the Arabian sea in May. Hence, in the absence of radiative forcing the ocean would cool down. The constant R_0 in the formula for the solar insolation was given the value $350 \times \pi$ so that the daily average irradiation is 350 W/m^2 and the maximum irradiation is 1099 W/m^2. All other parameters such as the turbulent Langmuir number, the Stokes drift decay length scale and the water friction velocity were chosen as in §4.1. Note that for these particular cases the decay length scale z_0 of the wave-induced stress and energy flux is assumed to be given by one-half the wind sea wave height.

In Fig. 12 time series of SST are shown over the five day period and are compared with a simulation without wave effects. Note that in the simulations without wave effects the wave dissipation term and the Langmuir term are switched off in the TKE equation (23), while also the wave-induced stress in the momentum equation (11) is switched off. The boundary condition for momentum flux at the surface is then, of course, replaced by the usual one, namely $\tau = -w_*^2$. Surprisingly, even for a low wind speed case of 2.5 m/s, sea state effects on the simulation of the diurnal cycle in SST are clearly visible. As expected, wave dissipation and Langmuir turbulence give rise to an enhanced mixing and therefore a reduction in the diurnal cycle amplitude compared to the case without wave effects. From the right panel of Fig. 12 a similar conclusion also follows for the diurnal cycle in the surface current. The corresponding amplitude is fairly substantial. Furthermore, note that while the time series for SST shows no drift in temperature or surface current in the simulation with waves, a drift is clearly visible in the simulation without waves. Presumably, in the simulation with waves there is a more efficient transport towards the deeper layers of the ocean.

In Fig. 13 profiles for turbulent velocity $Q(z)$, temperature $T(z)$ and velocity $u(z)$ are shown. Four hours into the simulation the ocean is warming up producing a stable layer as is evident from the fact that the turbulent velocity is less than 1 in the deeper parts of the ocean. Temperature and velocity profile are not in equilibrium because they have an S-shape. Eight hours later, at sunset, the upper part of the ocean is already turning unstable because the ocean is cooling off as the heatflux, given by $Q = -150$ W/m^2 is directed from ocean to atmosphere. Therefore, in the upper part of the ocean the temperature profile is well-mixed and is slightly lower at the surface than at $z/H_S \approx 6$ where the maximum temperature is found. The shape of the surface current is now concave and it looks similar to the equilibrium profiles shown in Fig. 10. Finally, at sunrise, 24 hours into the simulation the temperature in the whole column is almost uniform and equal to its value at the bottom of the domain. The reason is that during the night the whole ocean column becomes unstable giving an efficient transfer of heat towards the atmosphere and towards the deeper parts of the ocean. The efficient

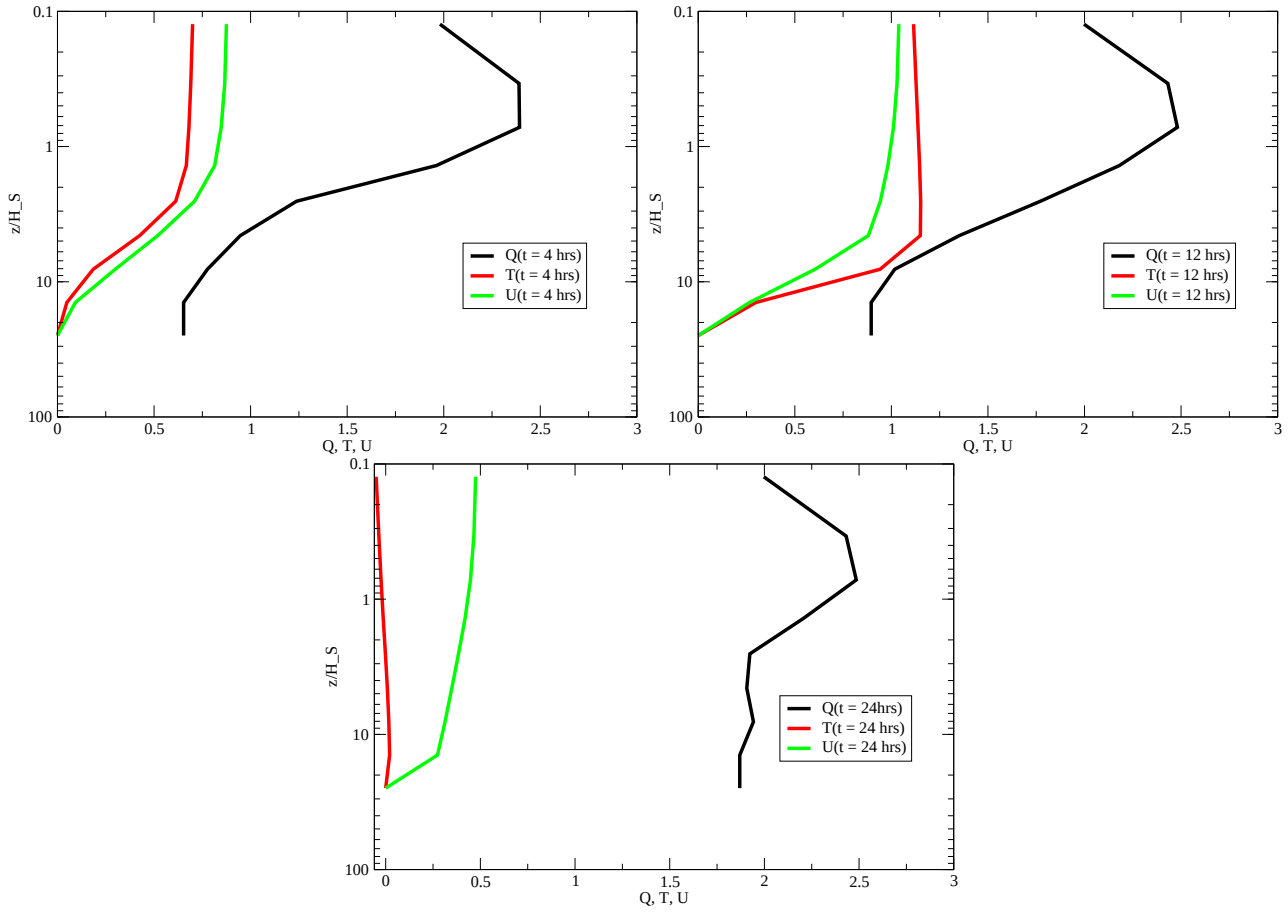

Figure 13: Profile of turbulent velocity, temperature and current after 4 (left), 12 (middle) and 24 (right) hours from the start of the simulation.

transfer is reflected by the observation that now the turbulent velocity is everywhere larger than 1. Furthermore, the current is now the smallest because during the night also momentum has been transferred efficiently towards the deep ocean.

In order to give an impression of the overall behaviour of the present mixed layer model a one-day simulation was performed for different wind speed and solar insolation. The results are summarized in Fig. 14. The plot shows that the amplitude in the diurnal cycle is a sensitive function of wind speed and the magnitude of the solar insolation. For comparison also shown is the wind speed dependence of the amplitude in diurnal cycle of SST when wave effects are switched off. In relative terms it is found that for low wind speed switching off the wave effects increases the diurnal amplitude by about 20% while for larger wind speed ($U_{10} > 5$ m/s) the increase is about 50%.

5.2 Simulation of buoy observations.

Next, a simulation with the mixed layer scheme is performed and validated against buoy observations of the Arabian Sea Mixed Layer Dynamics Experiment at 15^{o}30' N, 61^{o}30' E during a 3-month period from March to May 1995 (Baumgartner *et al.*, 1997; Weller *et al.*, 2002). The diurnal cycle of SST in the Arabian Sea can be quite profound. The mixed-layer model is driven by hourly surface fluxes computed with the COARE flux algorithm (Fairall *et al.*, 1996) using Improved Meteorology (IMET) buoy observations. Temperature

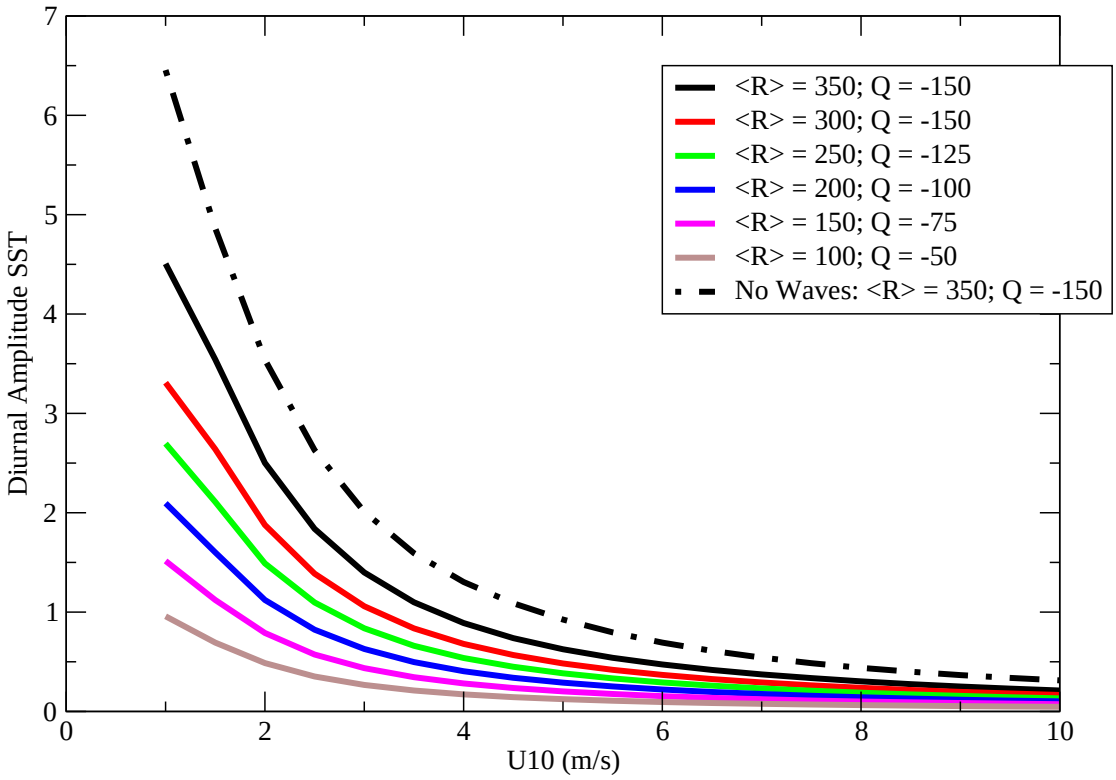

Figure 14: Diurnal amplitude in SST as function of wind speed for different solar insolation and heat flux as indicated in the legend. The sea state is pure windsea. For the most extreme case of insolation also the result in absence of wave effects is shown.In relative terms the difference is largest for large wind speed.

observations and flux data were downloaded from the Woods Hole Oceanographic Institution web page. For verification purposes observed temperature at a depth of 0.17 m are compared with the model counterpart. As a boundary condition the observed temperature at a depth of 3.5 m is prescribed, while the current at that depth is assumed to vanish. Sea state parameters such as significant wave height H_S, its wind sea part $H_{S,ws}$, the mean wavenumber k_S and the components of the Stokes drift are obtained from archived wave spectra from the ERA-Interim (wave) analysis (Simmons *et al.*, 2007). The 6-hourly wave parameters are interpolated in time and supplied to the mixed-layer scheme. However, as explained in §2, it is not straightforward to obtain the energy flux parameter α from archived spectra because the implicit factors of the integration scheme with which the energy balance equation (1) is solved need to be known. For this reason a parametrisation of Terray *et al.* (1996) is used. It is given by

$$\alpha = 15\chi \exp\left[-(0.04\chi)^4\right],$$

where $\chi = c_p/u_*$ is the wave age which characterizes the stage of development of the sea state. It is straightforward to obtain the wave age from archived spectra.

A number of experiments were performed with the present mixed-layer scheme. The first set of experiments were done to decide what is, in the context of the present model, the most appropriate penetration depth and/or roughness length z_0 that represents the transfer of ocean wave motion to ocean turbulence. A number of choices were tried, namely

1. relate z_0 to the inverse of a typical wavenumber such as the mean wavenumber k_S. This is the depth scale one would expect when the conversion from wave motion to ocean turbulence is described by potential theory.

2. relate z_0 to the wave height of the wind waves. This expresses the nonlinear character of the wave dissipation process.

3. relate z_0 to the significant wave height including swell. This reflects that the dissipating ocean waves are transported in the vertical by the longer waves.

The statistics from the comparison with the temperature observations are shown in Table 1 and it is clear that the third option performs best as the bias is very small while in particular the standard deviation of error in SST is only 0.12 K. Therefore, from now on the decay length scale will be given by $z_0 = 0.5H_S$ where H_S is the significant wave height which represents both windsea and swell. For this case a 20 day section of the timeseries for $\Delta T = T(0.17) - T(3.5)$ is shown in Fig. 15 while in Fig. 16 the modelled Diurnal SST Amplitude (DSA) is compared with the observed one. The mixed-layer model seems to perform remarkably well, and it is noted that the standard deviation of the difference between observed and modelled DSA is larger by about a factor of $\sqrt{2}$ since DSA is the difference between the daily maximum and minimum in SST.

Some additional experiments were performed. In §4.1 it was argued that the diffusion term in the TKE equation may probably be neglected. In order to verify this the mixed-layer model was run without diffusion in the TKE equation and the verification statistics were found to be almost identical to the case with diffusion (not shown) therefore confirming that neglect of diffusion in the TKE equation is a valid assumption. Furthermore, it is of interest to study the importance of Langmuir turbulence in the simulation of SST. Therefore, Langmuir turbulence was switched off and the resulting verification statistics are shown in Table 1 as well. It is seen that Langmuir turbulence has a relatively small impact on the simulation of the diurnal cycle for the present case. This can be understood by noting that for this particular example the average wavenumber over the three month period was found to be $< k_S > \approx 0.066$ so that the maximum contribution by Langmuir turbulence is

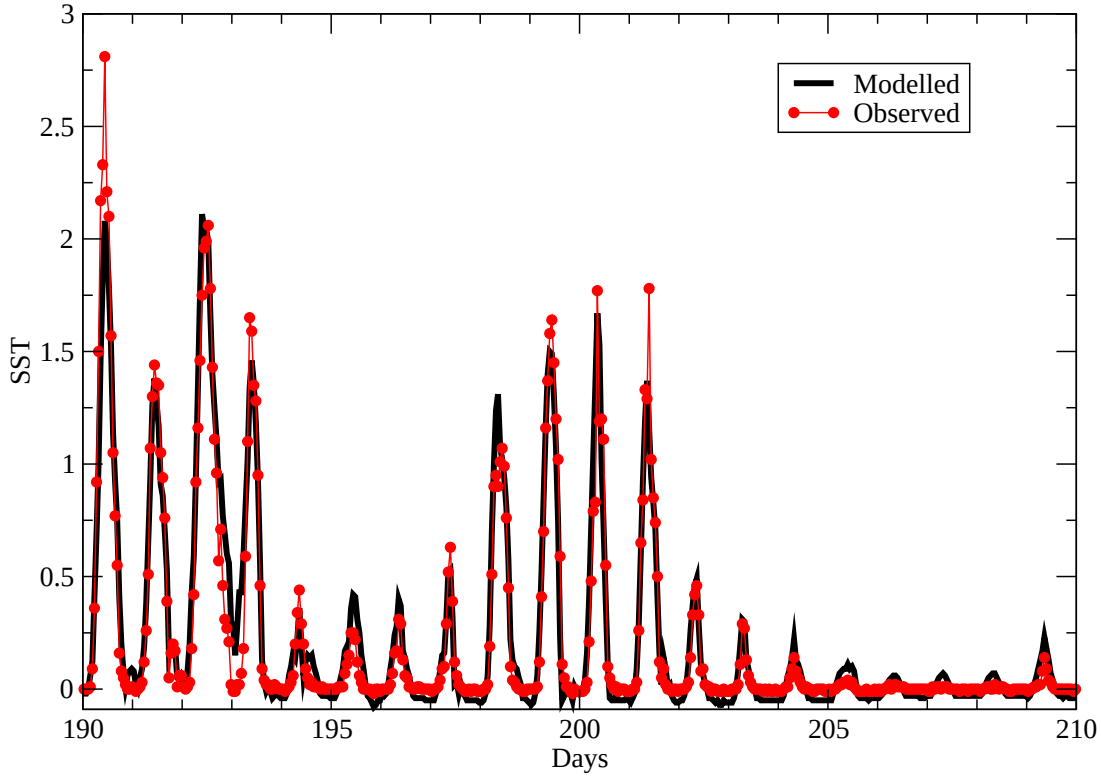

Figure 15: Observed and simulated ocean temperature $\Delta T = T(0.17) - T(3.5)$ at 15°30' N, 61°30' E in the Arabian Sea for 20 days from the 23rd of April.

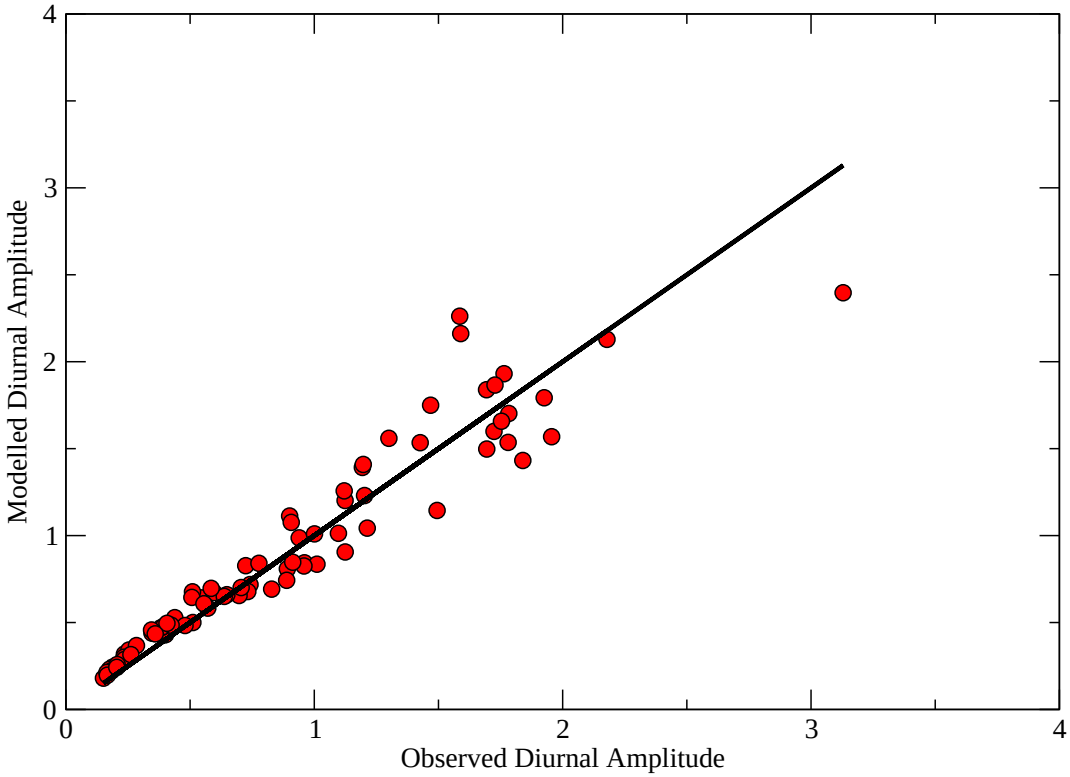

Figure 16: Comparison of simulated and observed diurnal amplitude at 15^{o}30' N, 61^{o}30' E in the Arabian Sea for the 3-month period starting from 1rst of March 1995.

at $z = 1/(2k_S) \approx 7.5$ m which is outside the domain that was modelled (recall that the boundary condition for temperature was provided at a depth of 3.5 m). A factor that has much more impact on the simulation results is how stratification effects are modelled. In order to illustrate the sensitivity to the shape of the stratification function f_M an experiment was performed where c_M in Eq. (55) is set to zero. In that event there is a critical Richardson number and, just like heat, momentum transport vanishes for large gradient Richardson number. As can be seen from Table 1 this change has a significant impact on the verification statistics, with a large increase in bias, standard deviation of error and normalized variability.

The final set of experiments explores the possible impact of waves on the simulation of the diurnal cycle. To that end, wave effects were switched off in the TKE equation while also the wave-induced stress term in the momentum equation was switched off. In this simulation, which is supposed to ignore wave effects, it makes no sense to relate the roughness length to the sea state. Therefore, after some trial and error optimizing statistics, the roughness length was given the value $z_0 = 1.5$ m which is close to a suggestion by Graig and Banner (1994). It is seen that also wave effects (and to be definite mainly wave dissipation) have a considerable impact on the SST simulation as the standard deviation errors increase by about 40-50 %. Additional evidence of the sensitivity of the diurnal cycle to the sea state may be found in the last two experiments. In the first one the average value of energy flux parameter α over the three month period is used in the wave dissipation term of the TKE equation. From Table 1 it is seen that this experiment gives almost the same statistics as the default experiment (indicated by the boldface numbers). However, if one would take in stead the global average of α, equal to 148, then the standard deviation of error in the DSA is seen to increase by 40% while variability is reduced by 25%. Hence, for an accurate simulation of the diurnal cycle an accurate representation of wave dissipation in space (and probably also in time) seems to be important. Returning to Fig. 3, which shows a measure of the normalized energy flux, it is seen that regarding wave dissipation the Arabian Sea is a very

Table 1: Summary of Statistics of a number of experiments. Here, DSA is the Diurnal SST Amplitude, SD is the standard deviation and VAR is the variability normalised with the observed variability. The number of hourly SST observations is 2040, while the number of daily cycles is 85.

Exp	Bias DSA	SD DSA	SST Bias	SD SST	VAR
$z_0 = 0.5H_{S,ws}$	+0.241	0.25	+0.078	0.19	1.32
$z_0 = 1/2k_S$	+0.153	0.20	+0.046	0.16	1.16
$z_0 = 0.5H_S$	**+0.022**	**0.18**	**+0.009**	**0.12**	**1.00**
No Langmuir	+0.029	0.18	+0.011	0.12	1.00
$c_M = 0$	+0.328	0.34	+0.110	0.24	1.41
No Waves	+0.053	0.25	-0.104	0.19	1.07
$\langle\alpha\rangle = 34$	+0.025	0.20	+0.008	0.13	1.01
$\langle\alpha\rangle = 148$	-0.172	0.26	-0.048	0.14	0.76

interesting area. In the western part high values of normalized wave dissipation are found, related to an active Somali jet generating steep waves, while in the eastern part of the Arabian Sea the sea state is much more gentle giving low values of α. The buoy used in the present simulation exercize was just located at the border of high and low values of normalized dissipation. Note that the Somali jet is intrinsically linked to the the onset of the Asian monsoon as it supplies the necessary moisture.

6 Conclusions.

The main purpose of this paper was to investigate the role of wave dissipation (e.g. wave breaking) and Langmuir turbulence on the mixing of the upper ocean. As an interesting first application the impact of ocean waves dynamics on the simulation of the diurnal cycle in SST was studied. The wave effects were studied in the context of the Mellor-Yamada (1982) scheme where the TKE equation was extended to allow for effects of wave dissipation and following Grant and Belcher (2009) effects of Langmuir turbulence. Following Janssen *et al.* (2004) effects of wave dissipation on turbulence production in the ocean column were incorporated by modelling the wave-induced energy flux $\overline{\delta p \delta w}$ while wave dissipation also affects the ocean momentum through the wave-induced stress. Particular attention was paid to modelling of stratification effects on the turbulent exchange coefficients for momentum, heat and turbulent kinetic energy, since, apart from solar insolation, the main reason for the existence of the diurnal cycle is the reduction of the turbulent transport by buoyancy effects. For low winds and strong solar forcing stratification in the ocean can become quite extreme, but unfortunately observations under these extreme circumstances are rare. Therefore, at least in the atmospheric context, there is no consensus on how the turbulent exchange coefficients behave in strongly stable conditions. First, it may be argued that turbulent motion is damped when the gradient Richardson number exceeds a critical value, say of the order of 1/4. A prominent example of this approach is the Mellor-Yamada scheme (1982). Many others argue, on the other hand, that beyond the critical Richardson number there is still transport possible related to internal gravity waves and intermittency. Presently, two directions may then be distinguished. One approach, which is based on observations, direct numerical simulations and group normalization methods argues that due to internal wave activity and intermittency momentum transfer will be more efficient than heat transport, while, on the other hand, from the SHEBA data there is compelling evidence that the opposite is true. A choice has therefore to be made, and in the main text arguments have been presented why I have chosen for the option of a more efficient momentum transport for the strongly stable case. At the same time, for the weakly stable case the proposed model for stratification agrees with the Kansas field experiment.

Properties of the resulting model for mixing in the upper ocean have been studied extensively. Under neutral circumstances it can be shown that the turbulent velocity may be obtained from a '1/3'-rule (see Eq. (44). This rule is important in understanding the sensitivity of upper ocean transport to variability in the sea state. When determining the energy flux from dissipating waves it is found that there is high variability in the dimensionless flux α in particular near the passage of a front (see Fig. 1). As the turbulent velocity depends, according to the '1/3'-rule only on $\alpha^{1/3}$, its variability, and the variability in the turbulent transport, is much reduced. The '1/3'-rule also explains that when only Langmuir turbulence is taking into account the turbulent velocity scales with $La^{-2/3}$ in agreement with the scaling arguments of Grant and Belcher (2009).

Results from a simulation with the present mixed layer model of the diurnal cycle in SST over a three month period for a location in the Arabian Sea are compared with in-situ observations and judged by statistical parameters such as bias, standard deviation and simulated variability there is an excellent agreement. It has also been shown that, as expected, results depend in a sensitive manner on the way stratification is modelled. For example, neglect of the contribution to turbulent transport by intermittency and internal gravity waves gives a large increase in error. In a similar spirit, it can be shown that wave effects play an important role in the mixing in the upper ocean. No sensitivity to Langmuir turbulence was found in the simulation results for the diurnal cycle, presumably because on average the maximum of the Langmuir production term was at a larger depth than the depth where the boundary condition for ocean temperature was given.

Nevertheless, the model still needs to be validated more extensively against satellite observations from geostationary satellites and polar orbiters. This work is left for the future.

Acknowledgements. Discussions with Yuhei Takaya and Anton Beljaars are greatly appreciated, while Jean Bidlot provided me with the sea state parameters from the ERA-interim reanalysis. I would also like to thank the Woods Hole Oceanographic Institution for making available the in-situ observations which were of great value in this model development.

7 References.

Abramowitz, M. and I.A. Stegun, 1964. *Handbook of Mathematical Functions*, Dover Publications, Inc., New York.

Anis, A. and J.N. Moun, 1995. Surface wave-turbulence interactions: Scaling $\varepsilon(z)$ near the sea surface. *J. Phys. Oceanogr.* **25**, 2025-2045.

Baas, P., S.R. de Roode and G. Lenderink, 2008. The Scaling Behaviour of a Turbulent Kinetic Energy Closure Model for Stably Stratified Conditions. *Boundary-Layer Meteorol.* **127**, 17-36.

Banner, M.L., 1990b. Equilibrium spectra of wind waves. *J. Phys. Oceanogr.* **20**, 966-984.

Baumgartner, M.F., N.J. Brink, W.M. Ostrom, R.P. Trask and R.A. Weller, 1997. Arabian Sea Mixed Layer Dynamics Experiment data report. *Woods Hole Oceanographic Institution Technical report WHOI-97-08*, UOP Technical Report 97-03, 157 pp.

Bidlot, J.-R., D.J. Holmes, P.A. Wittmann, R. Lalbeharry and H.S. Chen, 2002. Intercomparison of the Performance of Operational Ocean Wave Forecasting Systems with Buoy Data. *Weather and Forecasting* **17**, 287-310.

Birch, K.G. and J.A. Ewing, 1986. Observations of wind waves on a reservoir, IOS-rep. No. 234, Wormley, 37p.

Britter, R.E., J.C.R. Hunt, G.L. Marsh and W.H. Snyder, 1983. The effects of stable stratification on turbulent diffusion and the decay of grid turbulence. *J. Fluid Mech.* **127**, 27-44.

Burchard, H., 2001. Simulating the Wave-Enhanced Layer under Breaking Surface Waves with Two-Equation Turbulence Models. *J. Phys. Oceanogr.* **31**, 3133-3145.

Businger, J.A., J.C. Wyngaard, Y. Izumi and E.F. Bradley, 1971. Flux-Profile relationships in the Atmospheric Surface Layer. *J. Atmos. Sci.* **28**, 181-189.

Burgers, G.J.H., P.A.E.M. Janssen, and D.L.T. Anderson, 1995. Impact of sea-state dependent fluxes on the tropical ocean circulation. International Scientific Conference on the Tropical Ocean's Global Atmosphere (TOGAS), 2-7 April 1995, Melbourne, 295-297.

Cheng, Y. and W. Brutsaert, 2005. Flux-profile relationships for wind speed and temperature in the stable atmospheric boundary layer, *Boundary-Layer Meteorol.* **114**, 519-538.

Craig, P.D., 1996. Velocity profiles and surface roughness under breaking waves. *J. Geophys. Res.* **101**, 1265-1277.

Craig, P.D. and M.L. Banner, 1994. Modeling wave-enhanced turbulence in the ocean surface layer. *J. Phys. Oceanogr.* **24**, 2546-2559.

Csanady, G.T., 1964. Turbulent diffusion in a stratified fluid. *J. Atmos. Sci.* **21**, 439-447.

Deardorff, J.W., 1980. Stratocumulus-capped mixed layers derived from a three-dimensional model. *Boundary-Layer Meteorol.* **18** 495-527.

Drennan, W.M., M.A. Donelan, E.A. Terray and K.B. Katsaros, 1996. Ocean turbulence dissipation rate measurements in SWADE. *J. Phys. Oceanogr.* **26**, 808-815.

Fairall, C.W., E.F. Bradley, D.P. Rogers, J.B. Edson and G.S. Young, 1996. Bulk parametrization of air-sea

fluxes for Tropical Ocean-Global Atmosphere Coupled-Ocean Atmosphere Response Experiment. *J. Geophys. Res.* **101**, 3747-3764.

Grachev A.A., E.L. Andreas, C.W. Fairall, P.S. Guest and P.O.G. Persson, (2007a). SHEBA flux-profile relationships in the stable atmospheric boundary layer. *Boundary-Layer Meteorol.* **124** 315-333.

Grachev A.A., E.L. Andreas, C.W. Fairall, P.S. Guest and P.O.G. Persson, (2007b). On the turbulent Prandtl number in the stable atmospheric boundary layer. *Boundary-Layer Meteorol.* **125** 329-341.

Grant A.L.M. and S.E. Belcher, 2009. Characteristics of Langmuir Turbulence in the Ocean Mixed layer, *J. Phys. Oceanogr.* **39**, 1871-1887.

Hara T, and A.V. Karachintsev, 2003. Observation of Nonlinear Effects in Ocean Surface Wave frequency Spectra. *J. Phys. Oceanogr.* **33**, 422-430.

Hasselmann, K., T.P. Barnett, E. Bouws, H. Carlson, D.E. Cartwright, K. Enke, J.A. Ewing, H. Gienapp, D.E. Hasselmann, P. Kruseman, A. Meerburg, P. Müller, D.J. Olbers, K. Richter, W. Sell and H. Walden, 1973. Measurements of wind-wave growth and swell decay during the Joint North Sea Wave Project (JONSWAP), *Dtsch. Hydrogr. Z. Suppl. A* **8(12)**, 95p.

Janssen, P.A.E.M., 1999. On the effect of ocean waves on the kinetic energy balance and consequences for the inertial dissipation technique. *J. Phys. Oceanogr.* **29**, 530-534.

Janssen, P.A.E.M., O. Saetra, C. Wettre, H. Hersbach and J. Bidlot, 2004. Impact of the sea state on the atmosphere and ocean. Annales Hydrographiques 6e série, **3** (772), 31323.

Kim J. and L. Mahrt (1992) Simple formulation of turbulent mixing in the stable free atmosphere and nocturnal boundary layer. *Tellus* **44**, 381-394.

Komen, G.J., 1987. Energy and momentum fluxes through the sea surface. *Dynamics of the Ocean Surface Mixed Layer*, P. Müller and D. Henderson, Eds., Hawaii Institute of Geophysics Special Publications, 207-217.

Komen, G.J., L. Cavaleri, M. Donelan, K. Hasselmann, S. Hasselmann, and P.A.E.M. Janssen, 1994: *Dynamics and Modelling of Ocean waves* (Cambridge University Press, Cambridge)

Kondo J., O. Kanechika, N. Yasuda, 1978. Heat and momentum transfers under strong stability in the atmospheric surface layer. *J. Atmos. Sci.* **35**, 1012-1021.

Kondo, J., Y. Sasano and T. Ishii, 1979. On Wind-Driven Current and Temperature Profiles with Diurnal Period in the Oceanic Planetary Boundary Layer. *J. Phys. Oceanogr.* **9**, 360-372.

Large, W.G., J.C. McWilliams, and S.C. Doney, 1994. Oceanic vertical mixing: A review and a model with a nonlocal boundary parameterization. *Rev. Geophys.* **32**, 363-403.

Mellor, G.L. and T. Yamada, 1982. Development of a turbulence closure model for geophysical fluid problems. *Rev. Geophys. Space Phys.* **20**, 851-875.

Nieuwstadt, F.T.M., 1984. The turbulent structure of the stable, nocturnal boundary layer. *J. Atmos. Sci.* **41** 2202-2216.

Noh, Y. and H.J. Kim, 1999. Simulations of temperature and turbulence structure of the oceanic boundary layer with the improved near-surface process. *J. Geophys. Res.* **C104**, 15,621-15,633.

Panofsky, H.A., 1963. Determination of stress from wind and temperature measurements. *Quart. J. Roy. Meteor. Soc.*, **89**, 85-94.

Pacanowski, R.C. and S.G.H. Philander, 1981. Parameterization of Vertical Mixing in Numerical Models of

Tropical Oceans. *J. Phys. Oceanogr.* **11**, 1443-1451.

Phillips, O.M., 1977. The dynamics of the upper ocean, Cambridge University Press, Cambridge, 336p.

Plant, W.J., 1982. A relation between wind stress and wave slope. *J. Geophys. Res.* **C87**, 1961-1967.

Shih, L.H., J.R. Koseff, J.H. Ferziger and C.R. Rehmann, 2000. Scaling and parameterization of stratified homogeneous turbulent shear flow. *J. Fluid Mech.* **412**, 1.

Simmons, A., S. Uppala, D. Dee and S. Kobayashi, 2007. ERA-Interim: New ECMWF reanalysis products from 1989 onwards. *ECMWF Newsletter* **110**, pp. 25-35. European Centre for Medium-Range Weather Forecasts, Reading, U.K.

Soloviev, A.V., 1982. On the vertical structure of the ocean thin surface layer at light wind. *Dokl. Acad. Sci. USSR, Earth Sci. Ser., Engl. Transl.* **18**, 751-760.

Strang, E.J. and H.J.S. Fernando, 2001. Vertical mixing and transports through a stratified shear layer. *J. Phys. Oceanogr.* **31**, 2026-2048.

Sukoriansky, S., B. Galperin and I. Staroselsky, 2005. A quasinormal scale elimination model of turbulent flows with stable stratification. *Phys. Fluids* **17** 085107-1-28.

Terray, E.A., M.A. Donelan, Y.C. Agrawal, W.M. Drennan, K.K. Kahma, A.J. Williams, P.A. Hwang, S.A., and Kitaigorodskii, 1996. Estimates of Kinetic Energy Dissipation under Breaking Waves. *J. Phys. Oceanogr.* **26**, 792-807.

Terray, E.A., W.M. Drennan, and M.A. Donelan, 1999. The vertical structure of shear and dissipation in the ocean surface layer. *The wind-driven air-sea interface*, M.L. Banner, Ed., School of Mathematics, The University of New South Wales, Sydney, 239-245.

Weber, S.L., 1994. Statistics of the air-sea fluxes of Momentum and Mechanical energy in a Coupled wave-atmosphere model. *J. Phys. Oceanogr.* **24**, 1388-1398.

Weller, R.A., A.S. Fisher, D.L. Rudnick, C.C. Eriksen, T.D. Dickey, J. Marra, C. Fox and R. Leben, 2002. Moored observations of upper-ocean response to the monsoons in the Arabian Sea during 19941995, *Deep Sea Res., Part II*, **49**, 2195-2230.

Wyngaard, J.C., 1985. Structure of the planetary boundary layer and implications for its modeling. *J. Clim. Appl. Meterorol.* **24**, 1131-1142.

Zilitinkevich, S.S., T. Elperin, N. Kleeorin and I. Rogachevskii, 2007. Energy- and flux-budget (EFB) turbulence closure model for stably stratified flows. Part I: steady-state, homogeneous regimes. *Boundary-Layer Meteorol.* **125** 167-191.